# Middle Miocene calc-alkaline volcanism in Central Patagonia (47°S): petrogenesis and implications for slab dynamics

Felipe Espinoza, Diego Morata, Mireille Polve, Yves Lagabrielle, René C. Maury, Aude de la Rupelle, Christele Guivel, Joseph Cotten, Hervé Bellon, Manuel Suárez

*Andean Geology 37 (2): 300-328. July, 2010*

***Andean Geology***
*formerly Revista Geológica de Chile*
*www.scielo.cl/andgeol.htm*

# Middle Miocene calc-alkaline volcanism in Central Patagonia (47°S): petrogenesis and implications for slab dynamics

**Felipe Espinoza[1, 3*], Diego Morata[1], Mireille Polvé[2], Yves Lagabrielle[3], René C. Maury[4], Aude de la Rupelle[4], Christèle Guivel[5], Joseph Cotten[4], Hervé Bellon[4], Manuel Suárez[6]**

[1] *Departamento de Geología, Universidad de Chile, Casilla 13518, Correo 21, Santiago, Chile.*
*dmorata@cec.uchile.cl*

[2] *UMR-CNRS 5563 LMTG, Observatoire Midi-Pyrénées, Université Paul-Sabatier, 14 rue Edouard Belin, 31400 Toulouse, France.*
*polve@lmtg.obs-mip.fr*

[3] *UMR-CNRS 5234 Géosciences Montpellier, Université de Montpellier 2, CC 60, Place Eugène Bataillon, 34095 Montpellier Cedex 5, France.*
*yves.lagabrielle@gm.univ-montp2.fr*

[4] *UMR-CNRS 6538 Domaines océaniques, Université de Bretagne Occidentale, 6 avenue le Gorgeu, C.S. 93837, 29238 Brest Cedex 3, France.*
*rene.maury@univ-brest.fr; grolotte.aude@hotmail.fr; Jo.Cotten@univ-brest.fr; Herve.Bellon@univ-brest.fr*

[5] *UMR-CNRS 6112 Planétologie et Géodynamique, Université de Nantes, 2 rue de la Houssinière, B. P. 92208, 44322 Nantes Cedex 03, France.*
*christelle.guivel@univ-nantes.fr*

[6] *Servicio Nacional de Geología y Minería, Avenida Santa María 0104, Providencia, Santiago, Chile.*
*msuarez@sernageomin.cl*

* *Present address: Servicio Nacional de Geología y Minería, Avenida Santa María 0104, Providencia, Santiago, Chile.*
*fespinoza@sernageomin.cl*

**ABSTRACT.** We present a chronological (K-Ar), petrologic and geochemical study (major and trace elements, Sr-Nd isotopes) of Middle Miocene (*ca.* 16-14 Ma) calc-alkaline rocks (basalts to andesites) extruded in the present-day back-arc region of Central Patagonia (Zeballos Volcanic Sequence (ZVS), 47°S). This magmatism started shortly after mafic plutonism ceased in the arc region (*ca.* 16 Ma, 200 km west), and ended *ca.* 2 My before the onset of voluminous slab tear-related back-arc alkaline basaltic magmatism (*ca.* 12 to Pliocene). The studied calc-alkaline rocks have a typical subduction-related signature (high LILE/HFSE ratios, depletion in Nb, Ta and Ti; Ba/La >20; Ta/Hf <1.5; $(^{87}Sr/^{86}Sr)_o$=0.70366-0.70402, $\varepsilon_{Nd}$=+0.1-+3.8). Major and trace elements contents are consistent with their evolution by closed system fractional crystallization of a presumed parental liquid similar in composition to the most basic rock of the suite. Moreover, a strong subducted sediment imprint is recognized (increasing Th/HFSE and decreasing Ce/Pb during differentiation). However, these rocks show striking similarities with volcanic complexes emplaced above areas where a gently dipping slab occurs (high K contents; similar LREE/HREE, Nb/Zr, Ba/Nb; Th/Hf; Th/Ta, Ta/Hf<0.3), particularly the present-day Andean flat-slab region and the Neuquén Basin during the Late Miocene. A comprehensive tectono-magmatic model is here presented to explain the generation and extrusion of these calc-alkaline magmas during the Middle Miocene. The development of a transient low-angle subduction and the resulting eastward migration of the volcanic front are then proposed. Mixing between stored remnants of calc-alkaline magmatism and later primitive alkaline melts is envisioned as the most likely process accounting for the transitional signature (*i.e.*, intermediate between calc-alkaline and alkaline, La/Nb >1; $TiO_2$ <2 wt%) of some basalts extruded synchronously with genuine alkaline lavas in the Neogene Patagonian Plateau Lavas province.

*Keywords: Central Patagonia back-arc, Calc-alkaline magmatism, Low-angle subduction, Miocene.*

**RESUMEN. Volcanismo calcoalcalino durante el Mioceno Medio en Patagonia Central (47°S): petrogénesis e implicaciones en la dinámica de placas.** En este trabajo se presenta un estudio cronológico (K-Ar), petrológico y geoquímico (elementos mayores y trazas, isótopos de Sr-Nd) de rocas calcoalcalinas (basaltos a andesitas) del Mioceno Medio (16-14 Ma) que ocurren en una posición de trasarco en Patagonia Central (47°S; Secuencia Volcánica Zeballos, SVZ). Este magmatismo comenzó poco después de que el plutonismo máfico cesara en la región bajo el arco (*ca.* 16 Ma, 200 km al oeste), y terminó *ca.* 2 My antes del comienzo de un voluminoso evento magmático basáltico alcalino desarrollado en el trasarco, relacionado con ventanas astenosféricas, que continuó hasta el Pleistoceno. Las rocas calcoalcalinas estudiadas tienen una química típicamente relacionada con procesos de subducción (altas razones LILE/HFSE, empobrecimientos en Nb, Ta y Ti; Ba/La>20; Ta/Hf<1,5; $(^{87}Sr/^{86}Sr)_o$=0,70366-0,70402, $\varepsilon_{Nd}$=+0,1±3,8); y sus contenidos de elementos mayores y trazas son consistentes con una evolución por cristalización fraccionada, en un sistema cerrado, desde un líquido parental de composición similar a la de la roca más básica del conjunto analizado. Se reconoce, además, la influencia de sedimentos subductados en la composición de estos magmas (aumento de la razón Th/HFSE y disminución de la razón Ce/Pb durante la diferenciación). Sin embargo, estas rocas muestran importantes similitudes composicionales con las de complejos volcánicos emplazados sobre áreas donde ocurre subducción de bajo ángulo (altos contenidos de K, similares razones LREE/HREE, Nb/Zr, Ba/Nb; Th/Hf; Th/Ta, Ta/Hf<0,3), particularmente rocas de la actual región de subducción plana en Chile central-Argentina y de la cuenca de Neuquén durante el Mioceno Superior. Se propone aquí un modelo tectono-magmático que explica la generación y extrusión de magmas calcoalcalinos en una posición de trasarco durante el Mioceno Medio en Patagonia mediante el desarrollo de un fenómeno transiente de subducción de bajo ángulo y el consiguiente desplazamiento hacia el este del frente volcánico. Además, la mezcla entre remanentes de este magmatismo calcoalcalino almacenados en la corteza y fundidos alcalinos posteriores, provenientes de la astenósfera, se presenta como el proceso responsable de la generación de la signatura transicional (*i.e.,* intermedia entre calcoalcalina y alcalina, La/Nb>1; $TiO_2$<2 wt%) reconocida en algunos basaltos que ocurren contemporáneamente con otros puramente alcalinos en la provincia de las Lavas Neógenas de Plateau de la Patagonia.

*Palabras clave: Trasarco de Patagonia Central, Magmatismo calcoalcalino, Subducción de bajo ángulo, Mioceno.*

## 1. Introduction

The displacement of a volcanic arc front to regions behind a former arc and far away from the trench has been previously recognized in several regions. Moreover, diverse tectonomagmatic models have been proposed to explain this arc migration (Kay and Gordillo, 1994; Gutscher *et al.*, 2000; Beate *et al.*, 2001; Kay and Mpodozis, 2002; Bourdon *et al.*, 2003; Ramos and Folguera, 2009). This phenomenon is here proposed to have occurred during Early to Middle Miocene in Central Patagonia (47°S, Fig. 1) where calc-alkaline volcanic rocks were deposited above foreland sediments shortly after plutonism ceased in the early arc region.

The western border of the continent has been the site of oceanic subduction beneath the South American continental plate since the Jurassic. Miocene geological evolution of Patagonia was characterized by the occurrence of particular geodynamic and tectonic events, among them: **i)** the South Chile spreading ridge approached the Chile Trench and started to be subducted at *ca.* 15 Ma beneath the South American Plate at 55°S (Cande and Leslie, 1986), producing a northward progressing tearing of the subducted Nazca slab (Guivel *et al.*, 2006); **ii)** convergence parameters (angle and rate) between the Nazca and South American plates change (increasing velocity and oblique subduction (Pardo-Casas and Molnar, 1987; Somoza, 1998); **iii)** contractional deformation, although not well constrained in space and time, occurred in the Patagonian Fold and Thrust Belt (Ramos, 1989; Lagabrielle *et al.*, 2006) associated with **iv)** a topographic uplift of the chain (either by tectonic stacking or simple vertical uplift), and **v)** generation of molasse sediments, syntectonic plutonism and granite emplacement (Blisniuk *et al.*, 2005; Sánchez *et al.*, 2008). Until the Miocene, typical subduction-related arc magmatism generated the wide, trench-parallel, Patagonian Batholith. Early Miocene (22-16 Ma) calc-alkaline granitoids are present in its northern part (44°-47°S), but no volcanic products coeval with this plutonic activity have been described in the region. However, in the present-day back-arc region of the Central Patagonian Andes (~47-49°S, Fig. 1), ~200 km east from Miocene arc granitoids and more than 300 km from the Chile Trench, tuffaceous horizons (22 to 14 Ma, Blisniuk *et al.*, 2005) occur within Middle Miocene foreland continental sediments, and subvolcanic rocks of this age (including adakites) are also found. In the study area of El Zeballos valley (western border of

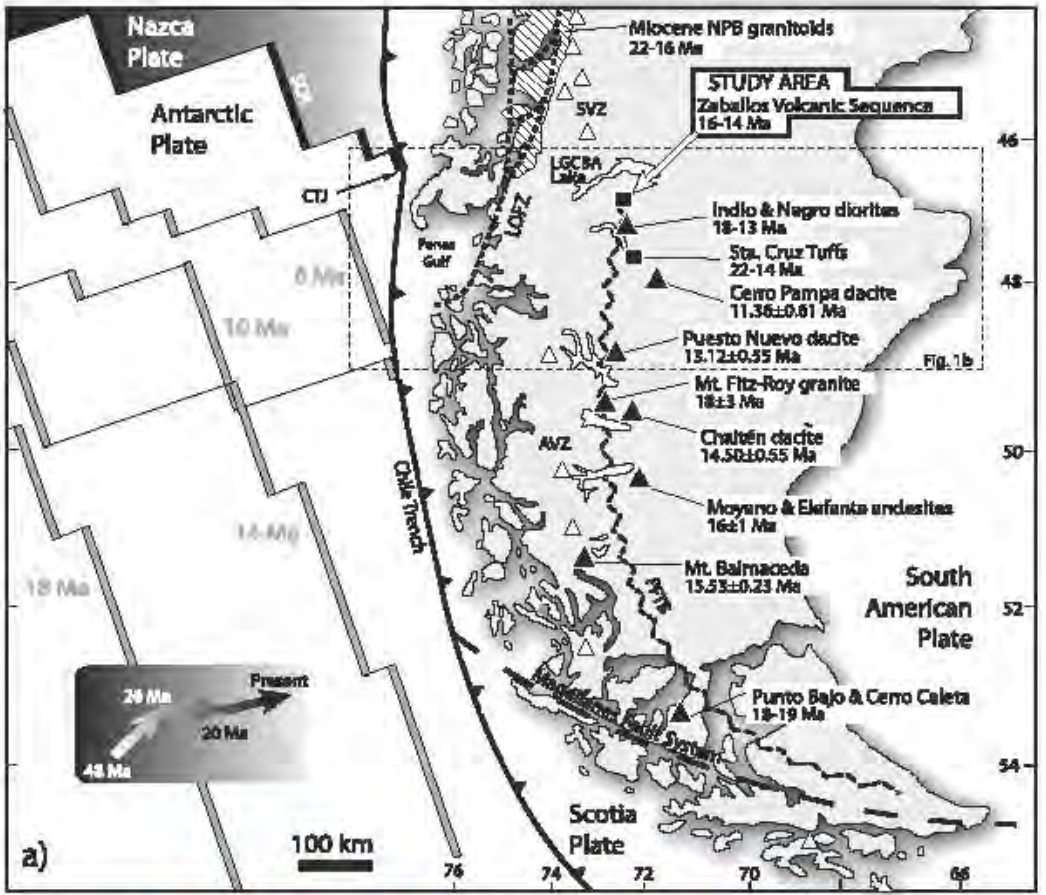
Nazca Plate
Antarctic Plate
CTJ
Chile Trench
Miocene NPB granitoids 22-16 Ma
STUDY AREA
Zaballos Volcanic Sequence 16-14 Ma
SVZ
LGCBA Lake
LOFZ
Penas Gulf
Indio & Negro diorites 18-13 Ma
Sta. Cruz Tuffs 22-14 Ma
Cerro Pampa dacite 11.36±0.61 Ma
Puesto Nuevo dacite 13.12±0.55 Ma
Fig. 1b
Mt. Fitz-Roy granite 18±3 Ma
AVZ
Chaltén dacite 14.50±0.55 Ma
Moyano & Elefante andesites 16±1 Ma
Mt. Balmaceda 15.53±0.23 Ma
PFTS
South American Plate
Punto Bajo & Cerro Caleta 18-19 Ma
Magallanes-Fagnano Fault System
Scotia Plate
Present
26 Ma
20 Ma
48 Ma
0 Ma
10 Ma
14 Ma
18 Ma
100 km
a)
46
48
50
52
54
76
74
72
70
66

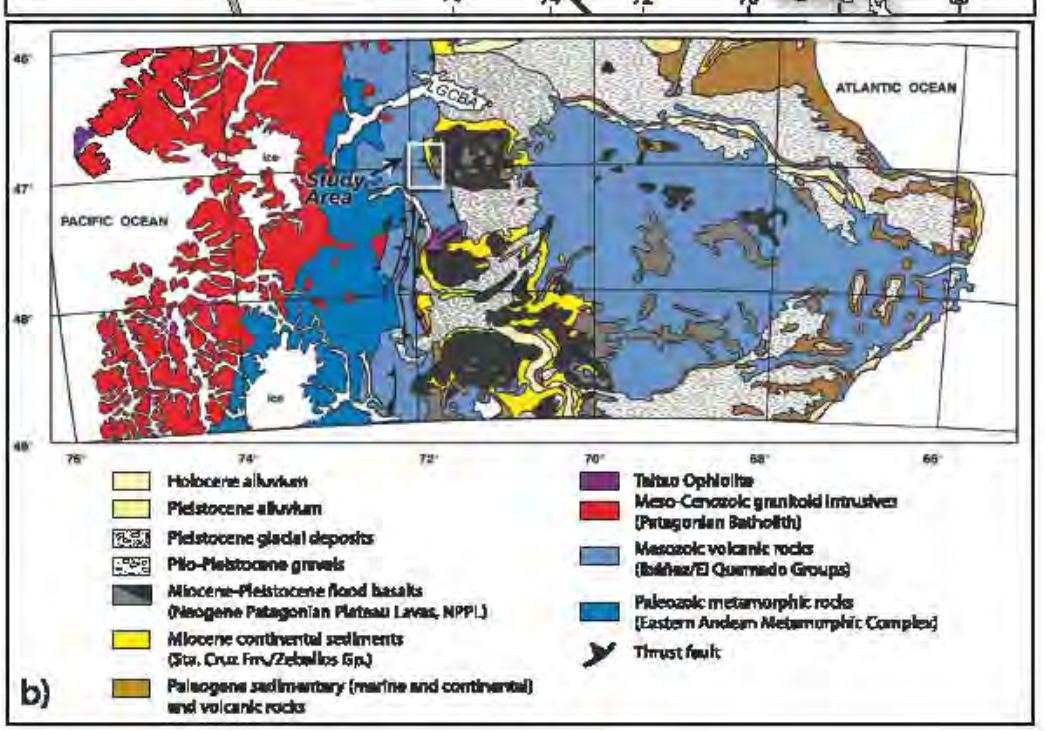
ATLANTIC OCEAN
PACIFIC OCEAN
LGCBA
Study Area
Ice
Ice
46°
47°
48°
49°
76°
74°
72°
70°
68°
66°
Holocene alluvium
Pleistocene alluvium
Pleistocene glacial deposits
Plio-Pleistocene gravels
Miocene-Pleistocene flood basalts (Neogene Patagonian Plateau Lavas, NPPL)
Miocene continental sediments (Sta. Cruz Fm./Zaballos Gp.)
Paleogene sedimentary (marine and continental) and volcanic rocks
Taitao Ophiolite
Meso-Cenozoic granitoid intrusives (Patagonian Batholith)
Mesozoic volcanic rocks (Bahías/El Quemado Groups)
Paleozoic metamorphic rocks (Eastern Andean Metamorphic Complex)
Thrust fault
b)

the Meseta del Lago Buenos Aires basaltic plateau) outcrops of Early to Middle Miocene volcanic rocks (basalts, basaltic andesites and andesites) overlie the synorogenic detrital sediments. The purpose of this paper is to discuss the nature of this magmatism, its relationships with the Early Miocene plutonism of the North Patagonian Batholith (NPB) and to explore a genetic link with the subduction of young oceanic plate beneath the continent at that time. In addition, we propose that this magmatism contributed as a geochemical end-member to the origin of the transitional signature observed in younger OIB-type basalts, particularly in the Meseta del Lago Buenos Aires basaltic plateau.

## 2. Geological Setting

The Aysén region in southern Chile (45º-48ºS) is characterized by the occurrence of the NPB adjacent to the Chile Trench (Figs. 1a, b), which forms the western and central areas of the Patagonian Cordillera. It corresponds to the northern part (north of the Golfo de Penas) of the Patagonian Batholith, a *ca*. 1,000 km long and 50-120 km wide belt of subduction-related plutonic rocks. The NPB, mostly consisting of metaluminous hornblende-biotite granodiorites (*e.g*., Pankhurst *et al*., 1999; Suárez and De la Cruz, 2001) has a well established zonal age pattern with Early Cretaceous margins and Cenozoic central portions. Early Miocene gabbros to granodiorites of the NPB crop out between 44º and 46ºS in the central part of the Batholith, ranging in age between 22-16 Ma (Pankhurst *et al*., 1999; Parada *et al*., 2000; Suárez and De la Cruz, 2001; Fig. 1a). According to Pankhurst *et al*. (1999), the wide compositional variation recognized in the batholith resulted from the contribution of a primitive subduction-related component stored underneath the continental crust (either as mafic magmas or underplated basalts) and that of an isotopically evolved end-member, here represented by the lower Patagonian crust. Simultaneous melting and magma-mixing relationships between these end-members, in proportions controlled by the subduction-related thermal regime, account for the complete range of rocks in the NPB. Intrusion and exhumation of these rocks were tectonically controlled during the Cenozoic by the continental-scale trench-parallel dextral strike-slip Liquiñe-Ofqui Fault Zone (Pankhurst *et al*., 1999; Cembrano *et al*., 2002; Thomson, 2002). The plutons intrude Paleozoic basement rocks (Eastern Andean Metamorphic Complex; Hervé, 1993; Bell and Suárez, 2000) and Jurassic to Late Cretaceous calc-alkaline volcanics and continental rocks (Ibáñez and Divisadero Group). In the studied region, these Mesozoic rocks form the eastern ranges of the Cordillera as thrust and folded blocks oriented N160-170 (Lagabrielle *et al*., 2004), defining the morphotectonic front of the chain.

The last orogenic phase of the Patagonian Andes occurred during the Late Miocene according to many authors (Ramos, 1989; Suárez *et al*., 2000; Thomson *et al*., 2001; Lagabrielle *et al*., 2004), and synorogenic foreland basin detrital products deposited in the present-day back-arc correspond to fine-to-coarse grained continental sandstones and conglomerates (Santa Cruz Formation and Zeballos Group; Ugarte, 1956; Marshall *et al*., 1986; Escosteguy *et al*., 2002). They crop out to the east in Argentina and in isolated intracordilleran basins (*e.g*., Cosmelli Basin; Flint *et al*., 1994), overlying the Mesozoic volcanics (Figs. 1b, 2a). The period of deposition of these sediments is well constrained between 22 and 14 Ma by dated

FIG. 1. **a.** Scheme of southern South America showing the location and ages of the Miocene calc-alkaline volcanic rocks occurring in the present-day back-arc region of Patagonia. Black squares: tuffs interbedded with the synorogenic deposits of Santa Cruz Formation and Zeballos Group; black triangles: intrusives (andesite porphyries, diorites, granites; Ramos, 2002; Ramos *et al.*, 2004); grey triangles: Patagonian adakites (Kay *et al.*, 1993; Ramos *et al.*, 2004); white triangles: actual volcanic arc edifices. Diagonal pattern: Lower Miocene North Patagonian Batholith (NPB) granitoids (Pankhurst *et al.*, 1999). Also shown the geometry of the Chile Ridge subduction along the continental border, black lines represent the present day position of the Chile Ridge segments under subduction at the Taitao Peninsula, grey lines represents past location of the Chile Ridge segments at 6 Ma, 10 Ma, 14 Ma and 18 Ma. Arrows indicate the convergence vector for Nazca Plate since 48 Ma (after Cande and Leslie, 1986; Pardo-Casas and Molnar, 1987; Somoza, 1998; Breitsprecher and Thorkelson, 2009). Location of Fig. 1b is shown by a frame; **b**. Regional geological map of the Aysén Region (Chile) and Santa Cruz Province (Argentina). The precise location of the study area is indicated. Location of the detailed stratigraphic section of the Santa Cruz Formation by Blisniuk *et al.* (2005) is indicated by a fuchsia arrow. **LOFZ:** Liquiñe-Ofqui Fault Zone; **PFTB:** Patagonian Fold and Thrust Belt; **SVZ:** Southern Volcanic Zones; **AVZ:** Austral Volcanic Zone; **SCR:** South Chile Ridge; **CTJ:** Chile Triple Junction; **LGCBA:** Lago General Carrera-Buenos Aires.

tuffaceous horizons interbedded with the sediments (Feagle *et al.*, 1995; Marshall *et al.*, 1986; Blisniuk *et al.*, 2005). This depositional phase was sealed by a major final contractional tectonic event, leading to the development of the main Cordillera frontal thrust between 14.5 and ~12 Ma (Lagabrielle *et al.*, 2004, 2006). Other records of Early to Middle Miocene volcanic activity in Central Patagonia correspond to scarce calc-alkaline subvolcanic bodies recognized close to the studied area (Cerro Negro del Ghío and Cerro Indio diorites; Ramos, 2002) and as far as 390 km south (Cerro Moyano and Cerro Elefante andesitic porphyries; Linares and González, 1990), together with three Middle Miocene adakitic dacites (Cerro Pampa, Chaltén and Puesto Nuevo; Kay *et al.*, 1993; Ramos *et al.*, 2004), occurring also in a back-arc position (Fig. 1a; Table 1). Other calc-alkaline rocks occur further south but close to the arc position (Cerro Blamaceda: 15.43 0.23 Ma U-Pb, Sánchez *et al.*, 2006 and Sánchez, 2010, personal communication; Punto Bajo hornblende andesite flow: 18.3 0.6 Ma, and Cerro Caleta granodiorite sill: 19.7 0.6 Ma; Morello *et al.*, 2001).

The foreland sediments are locally unconformably overlain by Late Miocene-Early Pliocene alkaline basalts derived from the subslab asthenosphere (the Neogene Patagonian Plateau Lavas (NPPL) basaltic province *e.g.*, Gorring *et al.*, 1997; Fig. 1b). Geodynamic models suggest that these primitive partial melts ascended through a tear in the slab (Guivel *et al.*, 2006) opened in the Nazca Plate in response to the Chile Ridge subduction at 55°S, starting at

**TABLE 1. WHOLE ROCK K-Ar AGES OF ROCKS OF THE ZEBALLOS VOLCANIC SEQUENCE.**

| Sample | Rock type | Dated Material | Sequence location | $K_2O$ (wt%) | $^{40}Ar_R$ (%) | $^{36}Ar$ $e^{-9}cm^3g^{-1}$ | Age (Ma) | ± Error (2σ) |
|---|---|---|---|---|---|---|---|---|
| PAT-36 | Basalt | Whole-rock | Zeballos hill | 1.18 | 58.5 | 1.07 | 14.5 | ± 0.7 |
| PAT-32 | Trachy-andesite | Whole-rock | Zeballos hill | 3.12 | 72.9 | 1.50 | 14.8 | ± 0.7 |
| PAT-37 | Bas. Andesite | Whole-rock | Zeballos hill | 1.75 | 70.8 | 0.95 | 15.0 | ± 0.7 |
| PAT-33 | Bas. Andesite | Whole-rock | Zeballos hill | 1.98 | 71.6 | 1.15 | 16.5 | ± 0.8 |
| **Blisniuk *et al.* (2005); Ar/Ar total fusion in feldspar** | | | | | | | | |
| LP-I>504.5 | Tuff | Feldspar | South Lago Posadas | - | - | - | 14.24 | ± 0.78* |
| LP 331.5 | Tuff | Feldspar | South Lago Posadas | - | - | - | 15.51 | ± 0.41* |
| LP 251.7 | Tuff | Feldspar | South Lago Posadas | - | - | - | 16.45 | ± 0.25* |
| LP 181.2 | Tuff | Feldspar | South Lago Posadas | - | - | - | 16.71 | ± 0.63* |
| LP 58.8 | Tuff | Feldspar | South Lago Posadas | - | - | - | 18.15 | ± 0.31* |
| LP 10.0 | Tuff | Feldspar | South Lago Posadas | - | - | - | 22.36 | ± 0.36* |
| **Ramos (2002); whole-rock K-Ar** | | | | | | | | |
| Cerro Indio | Diorite | Whole-rock | Zeballos valley | - | - | - | 13.2 | ± 0.9 |
| Cerro Negro del Ghío | Diorite | Hornblende | Zeballos valley | - | - | - | 18.1 | ± 1.2 |
| Cerro Negro del Ghío | Diorite | Whole-rock | Zeballos valley | - | - | - | 15.8 | ± 0.7 |
| Cerro Negro del Ghío | Diorite | Whole-rock | Zeballos valley | - | - | - | 15.8 | ± 0.6 |
| | | | | - | - | - | | |
| **Linares and González (1990); whole-rock K-Ar** | | | | | | | | |
| Cerro Moyano | Andesite porph. | Whole-rock | South Lago Argentino | - | - | - | 16.0 | ± 1.0 |
| **Ramos *et al.* (2004); step heating $^{40}Ar/^{39}Ar$** | | | | | | | | |
| Cerro Pampa | Dacite | Hornblende | Pampa del Asador | - | - | - | 11.79 | ± 0.96 |
| Cerro Pampa | Dacite | Whole-rock | Pampa del Asador | - | - | - | 12.54 | ± 0.63 |
| Puesto Nuevo | Dacite | Hornblende | Lago San Martín | - | - | - | 12.97 | ± 1.14 |
| Puesto Nuevo | Dacite | Whole-rock | Lago San Martín | - | - | - | 13.08 | ± 0.76 |
| Chaltén | Dacite | Hornblende | East Mt. Fitz Roy | - | - | - | 14.67 | ± 0.34 |

Ages of contemporaneous rocks occurring in Central Patagonia are also listed.

Decay constant: $\lambda_Z=0.581\times10^{-10}yr^{-1}$; $\lambda_\beta=4.96\times10^{-10}yr^{-1}$; $^{40}K/K_{total}=0.0167$

(*) 1σ age uncertainties

*ca.* 15 Ma (Cande and Leslie, 1986). Notably, and particularly in the Meseta del Lago Buenos Aires (MLBA) and Meseta Chile Chico (MCC) plateaux, this basaltic sequence ('main-plateau' stage: 12.18-3.32 Ma, Guivel *et al.*, 2006) includes both pure OIB-type alkaline basalts and transitional basalts. The geochemical signature of the latter is intermediate between alkaline and calc-alkaline magmas (La/Nb>1; $TiO_2$<2 wt%; Stern *et al.*, 1990; Gorring *et al.*, 1997, 2003; Gorring and Kay, 2001; Espinoza *et al.*, 2005; Guivel *et al.*, 2006). Younger Plio-Pleistocene 'post-plateau' bimodal magmatism shows typical alkaline signatures. It includes primitive basanitic melts which rose through a completely opened slab window (Gorring *et al.*, 2003) and were later stored, contaminated and differentiated in shallow crustal reservoirs (Espinoza *et al.*, 2008).

### 2.1. Field observations and sampling in Cerro Zeballos

The analyzed samples were collected from the top of Cerro Zeballos (1,900 m a.s.l.), a remnant relief located in the middle of the glacial valley of El Zeballos/Alto Ghío rivers. This valley coincides with the N160-170 Zeballos Fault Zone which defines here the morphotectonic front of the Cordillera (Lagabrielle *et al.*, 2004, 2006), and shows evidence of Pliocene extensional tectonics (Lagabrielle *et al.*, 2007) which in tun may explain the young morphology of Cerro Zeballos (Figs. 2a, 3a). The base of this hill consists of synorogenic sandstones and conglomerates of the Zeballos Group, characteristically cross-cut by a network of east-west-striking basaltic dikes which likely represent the feeders of the overlying MLBA lava flows. Towards the summit, the conglomerates crop-out as thick layers forming steep cliffs (Fig. 3a). The studied volcanic sequence (Zeballos Volcanic Sequence, ZVS; Figs. 2 and 3), *ca.* 25 m thick, rests unconformably over the sediments, forming the top of the hill. The ZVS includes a lower 10-12 m thick whitish andesitic flow bearing centrimetric amphibole phenocrysts, and the overlying upper dark-grey olivine basaltic flow, also 10-12 m thick, which shows a well-preserved scoriaceous surface (Fig. 3b; samples PAT-37 and PAT-36, respectively). Several blocks of local origin (~4 m in diameter) of coarse chaotic to well-bedded breccia (debris flow-type) occur on the gentle south slope of the hill (Figs. 3a, c, d). Rock fragments forming these blocks are metric and angular in the coarse layers and centimetric and well rounded in the stratified horizons, and are set in coarse and fine volcaniclastic granular matrixes, respectively. They are compositionally homogeneous and similar to the andesitic deposit (no basaltic fragments were recognized) (Figs. 3c, d). Two of these fragments were separated for dating and chemical analysis (PAT-32 & -33). Based on these observations, good stratigraphic correlations can be made between the ZVS rocks and a detailed column of the Sta. Cruz Formation measured ~65 km south of the study area by Blisniuk *et al.* (2005) (Fig. 2b). A rounded boulder of fresh porphyritic andesite collected in the surroundings of Cerro Zeballos was also analyzed (PAT-39). Commonly, these andesite boulders contain centimetric to decimetric rounded amphibole- and plagioclase-rich gabbroic nodules (Fig. 5a), one of which was separated for analysis (PAT-38X). Finally, an isolated block (probably ice-transported) of fresh porphyritic andesite (PAT-26) was collected at 2,000 m altitude, east from Cerro Zeballos, on the western scarps of the MLBA.

## 3. Analytical methods

Whole rock $^{40}K$-$^{40}Ar$ ages were obtained at the Université de Bretagne Occidentale (Brest, France) geochronology laboratory. Analyses were performed on the 0.5- to 0.15 mm-size fraction after crushing, sieving and cleaning with distilled water of whole-rock samples. One aliquot of sample was powdered for K analysis by atomic absorption after HF chemical dissolution and 0.5-0.15-mm grains were used for argon isotopic analyses. Argon extraction was performed by the direct technique under high vacuum (10-5–10-7 hPa) using induction heating of a molybdenum crucible. The argon content was measured by isotope dilution and argon isotopes were analyzed in an 1808-geometry stainless steel mass spectrometer, according to the original procedure described by Bellon *et al.* (1981). Age calculations, following the equation of Mahood and Drake (1982) and using the constants recommended by Steiger and Jäger (1977), are given, with 2σ error, in table 1.

Mineral chemistry (Table 2) was carried out at Microsonde Sud (Montpellier, France), using a five spectrometer Probe CAMEBAX SX-100 and at LMTG (Toulouse, France) using a three spectrometer Probe CAMEBAX SX-50. Analytical conditions were 10 nA,

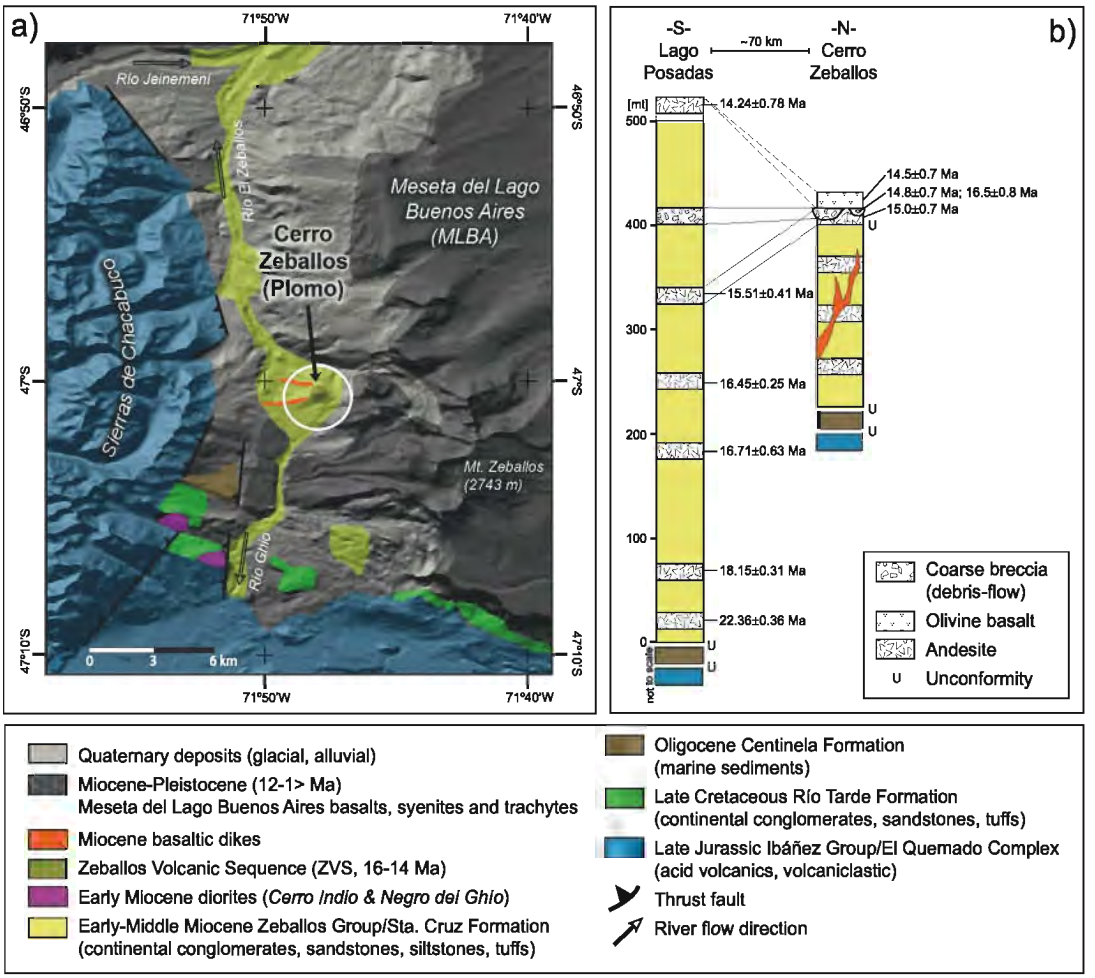


FIG. 2. **a.** Local geological map colored over the Digital Elevation Model (DEM, SRTM2 90 m) of the study area; location of Cerro Zeballos (also known as Cerro Plomo) is shown by a circle. Note its isolated occurrence in the Portezuelo area, which marks the divide in river's flow direction (indicated by empty arrows); **b.** Stratigraphic columns showing correlations between a 500 m detailed section of Santa Cruz Formation from Blisniuk *et al.* (2005) near Posadas Lake, and a generalized stratigraphic column of the Zeballos Volcanic Sequence at Cerro Zeballos. Ages of dated rocks in both localities are shown. See exact location of Blisniuk *et al.*'s work in figure 1b.

15-20 kV, using natural standards as reference and ZAF corrections in both probes. A detailed account of the procedure is given in Defant *et al.* (1991).

All major and selected trace element analyses (Sc, V, Cr, Co, Ni, Zr) (Table 3) were performed on agate-ground powders by ICP-AES at the chemical laboratory of the Université de Bretagne Occidentale (Brest, France). All data were measured using IWG-GIT, BE-N, AC-E, PM-S and WS-E as standards. Specific details for the analytical methods and sample preparation can be found in Cotten *et al.* (1995).

Trace element analyses of the other five samples (Table 3) were performed by ICP-MS using an Elan 6000 Perkin Elmer quadripolar ICP-MS at the LMTG (Toulouse, France). Calibrations, internal standard and interferences corrections were done following the procedure described in Aries *et al.* (2000). Data quality was controlled by running BCR-2 standard. Relative standard deviations are generally ≤5%.

The Sr and Nd isotopic compositions of five selected samples (Table 4) were analyzed on a Finnigan-Mat 261 multicollector mass spectrometer

**TABLE 2. REPRESENTATIVE EMPA MINERAL CHEMISTRY ANALYSES OF ROCKS OF THE MIOCENE ZEBALLOS VOLCANIC SEQUENCE.**

| **Mineral** | **Olivine** | | **Pyroxene** | | | | | | **Plagioclase** | | | | | | **Hornblende** | | | |
|---|---|---|---|---|---|---|---|---|---|---|---|---|---|---|---|---|---|---|
| **Sample** | **PAT-36** | **PAT-36** | **PAT-38A** | **PAT-38A** | **PAT-36** | **PAT-36** | **PAT-26** | **PAT-26** | **PAT-38A** | **PAT-38A** | **PAT-36** | **PAT-36** | **PAT-37** | **PAT-37** | **PAT-38A** | **PAT-38A** | **PAT-26** | **PAT-37** |
| **Rock** | **Basalt** | **Basalt** | **Gabbro** | **Gabbro** | **Basalt** | **Basalt** | **Andesite** | **Andesite** | **Gabbro** | **Gabbro** | **Basalt** | **Basalt** | **Andesite** | **Andesite** | **Andesite** | **Gabbro** | **Andesite** | **Andesite** |
| **No. analysis** | **27** | **54** | **5** | **14** | **11** | **15** | **79** | **71** | **2** | **4** | **46** | **48** | **2** | **68** | **70** | **107** | **140** | **54** |
| **Obs.** | **rim** | **core** | | | **rim** | **core** | **core** | **MF** | | | | | | | | | | |
| $SiO_2$ | 37.12 | 37.34 | 51.67 | 51.34 | 50.69 | 49.65 | 52.52 | 49.11 | 45.05 | 46.88 | 46.11 | 49.99 | 61.09 | 43.69 | 41.65 | 42.74 | 41.79 | 40.85 |
| $TiO_2$ | 0.07 | 0.03 | 0.20 | 0.07 | 0.96 | 0.69 | 0.31 | 0.89 | 0.00 | 0.00 | 0.00 | 0.09 | 0.04 | 0.01 | 3.08 | 1.78 | 2.58 | 2.56 |
| $Al_2O_3$ | 0.05 | 0.03 | 1.70 | 1.23 | 2.92 | 4.62 | 2.35 | 3.90 | 34.36 | 32.84 | 33.54 | 30.69 | 24.98 | 35.45 | 11.47 | 10.56 | 13.62 | 13.18 |
| FeO | 32.74 | 27.99 | 9.14 | 10.21 | 11.59 | 4.65 | 15.97 | 9.56 | 0.22 | 0.48 | 0.65 | 0.63 | 0.58 | 0.46 | 14.16 | 15.74 | 8.03 | 13.08 |
| MnO | 0.64 | 0.54 | 0.71 | 0.72 | 0.32 | 0.06 | 0.31 | 0.23 | 0.00 | 0.00 | 0.00 | -0.00 | 0.02 | -0.00 | 0.45 | 0.45 | 0.06 | 0.30 |
| MgO | 28.42 | 33.51 | 12.89 | 11.25 | 11.35 | 14.72 | 26.35 | 12.58 | 0.00 | 0.00 | 0.05 | 0.09 | 0.04 | 0.00 | 11.96 | 11.09 | 15.56 | 12.50 |
| CaO | 0.56 | 0.50 | 22.73 | 22.95 | 21.33 | 23.84 | 1.41 | 23.37 | 18.93 | 17.10 | 17.55 | 14.42 | 6.06 | 19.28 | 11.83 | 11.90 | 12.15 | 12.17 |
| $Na_2O$ | 0.03 | 0.03 | 0.32 | 0.33 | 0.53 | 0.21 | 0.01 | 0.29 | 0.84 | 1.77 | 1.64 | 3.45 | 6.58 | 0.68 | 2.33 | 2.41 | 2.18 | 2.57 |
| $K_2O$ | 0.00 | -0.00 | 0.00 | 0.01 | 0.06 | 0.00 | 0.00 | 0.00 | 0.00 | 0.00 | 0.12 | 0.39 | 1.40 | 0.02 | 1.19 | 1.21 | 1.31 | 0.90 |
| NiO | 0.05 | 0.01 | 0.09 | 0.00 | 0.02 | 0.00 | 0.00 | 0.00 | 0.00 | 0.00 | -0.00 | 0.03 | 0.00 | 0.00 | 0.04 | 0.00 | 0.03 | 0.00 |
| $Cr_2O_3$ | 0.00 | 0.01 | 0.05 | 0.00 | 0.00 | 0.82 | 0.00 | 0.05 | 0.00 | 0.00 | 0.01 | 0.01 | 0.00 | 0.00 | 0.01 | 0.03 | 0.10 | 0.00 |
| Total | 99.66 | 99.99 | 99.51 | 98.11 | 99.77 | 99.26 | 99.23 | 99.98 | 99.39 | 99.07 | 99.66 | 99.79 | 100.78 | 99.58 | 98.15 | 97.93 | 97.41 | 98.10 |
| Si | 1.021 | 1.001 | 1.943 | 1.975 | 1.918 | 1.837 | 1.910 | 1.836 | 2.094 | 2.177 | 2.137 | 2.297 | 2.705 | 2.035 | 6.202 | 6.425 | 6.071 | 6.043 |
| Ti | 0.001 | 0.001 | 0.006 | 0.002 | 0.027 | 0.019 | 0.009 | 0.025 | 0.000 | 0.000 | 0.000 | 0.003 | 0.001 | 0.000 | 0.344 | 0.201 | 0.282 | 0.285 |
| Al | 0.001 | 0.001 | 0.075 | 0.056 | 0.130 | 0.202 | 0.101 | 0.172 | 1.882 | 1.797 | 1.832 | 1.662 | 1.303 | 1.946 | 2.014 | 1.871 | 2.331 | 2.297 |
| $Fe^{2+}$ | 0.753 | 0.628 | 0.240 | 0.314 | 0.347 | 0.069 | 0.426 | 0.177 | 0.009 | 0.019 | 0.025 | 0.024 | 0.021 | 0.018 | 1.622 | 1.912 | 0.764 | 1.402 |
| $Fe^{3+}$ | - | - | 0.049 | 0.015 | 0.021 | 0.076 | 0.062 | 0.125 | - | - | - | - | 0.000 | 0.000 | 0.141 | 0.067 | 0.211 | 0.216 |
| $Mn^{2+}$ | 0.015 | 0.012 | 0.023 | 0.023 | 0.010 | 0.002 | 0.009 | 0.007 | 0.000 | 0.000 | 0.000 | 0.000 | 0.001 | 0.000 | 0.056 | 0.058 | 0.007 | 0.037 |
| Mg | 1.166 | 1.339 | 0.722 | 0.645 | 0.640 | 0.812 | 1.429 | 0.701 | 0.000 | 0.000 | 0.003 | 0.006 | 0.003 | 0.000 | 2.655 | 2.486 | 3.369 | 2.757 |
| Ca | 0.017 | 0.014 | 0.916 | 0.946 | 0.865 | 0.945 | 0.055 | 0.936 | 0.943 | 0.851 | 0.872 | 0.710 | 0.287 | 0.962 | 1.887 | 1.917 | 1.890 | 1.929 |
| Na | 0.002 | 0.001 | 0.023 | 0.024 | 0.039 | 0.015 | 0.001 | 0.021 | 0.076 | 0.160 | 0.147 | 0.307 | 0.565 | 0.061 | 0.672 | 0.702 | 0.614 | 0.738 |
| K | 0.000 | 0.000 | 0.000 | 0.000 | 0.003 | 0.000 | 0.000 | 0.000 | 0.000 | 0.000 | 0.007 | 0.023 | 0.079 | 0.001 | 0.226 | 0.233 | 0.243 | 0.171 |
| Ni | 0.001 | 0.000 | 0.003 | 0.000 | 0.001 | 0.000 | 0.000 | 0.000 | 0.000 | 0.000 | 0.000 | 0.000 | 0.000 | 0.000 | 0.005 | 0.000 | 0.004 | 0.000 |
| $Cr^{3+}$ | 0.000 | 0.000 | 0.002 | 0.000 | 0.000 | 0.024 | 0.000 | 0.002 | 0.000 | 0.000 | 0.000 | 0.000 | 0.000 | 0.000 | 0.001 | 0.003 | 0.012 | 0.000 |
| Sum | 2.978 | 2.998 | 4.001 | 4.000 | 4.001 | 4.001 | 4.003 | 4.003 | 5.003 | 5.004 | 5.024 | 5.033 | 4.964 | 5.023 | 15.825 | 15.875 | 15.798 | 15.875 |
| mg# | - | - | 0.75 | 0.67 | 0.65 | 0.92 | 0.77 | 0.80 | - | - | - | - | - | - | - | - | - | - |
| En (Fo) | 0.61 | 0.68 | 37.05 | 33.19 | 34.02 | 42.65 | 72.11 | 36.03 | - | - | - | - | - | - | - | - | - | - |
| Fs (Fa) | 0.39 | 0.32 | 15.97 | 18.14 | 20.05 | 7.70 | 25.12 | 15.88 | - | - | - | - | - | - | - | - | - | - |
| Wo | - | - | 46.97 | 48.67 | 45.93 | 49.64 | 2.77 | 48.09 | - | - | - | - | - | - | - | - | - | - |
| An | - | - | - | - | - | - | - | - | 92.58 | 84.20 | 84.97 | 68.31 | 30.86 | 93.91 | - | - | - | - |
| Ab | - | - | - | - | - | - | - | - | 7.42 | 15.80 | 14.36 | 29.52 | 60.65 | 5.96 | - | - | - | - |
| Or | - | - | - | - | - | - | - | - | 0.00 | 0.00 | 0.68 | 2.17 | 8.49 | 0.13 | - | - | - | - |

Cation per formula unit of representative olivine based on 4 Ox, pyroxenes on 6 Ox, plagioclase on 8 Ox and hornblende on 23 Ox.

**TABLE 3. REPRESENTATIVE GEOCHEMICAL ANALYSES OF MIOCENE CALC-ALKALINE ROCKS OF THE ZEBALLOS VOLCANIC SEQUENCE.**

| Sample | PAT 26 | PAT 32 | PAT 33* | PAT 36 | PAT 37 | PAT 38 | PAT 39* |
|---|---|---|---|---|---|---|---|
| Age [Ma] | | 14.8 | 16.5 | 14.5 | 15.0 | - | - |
| UTM | 290,427/ 4,789,707 | 286,986/ 4,790,211 | 286,986/ 4,790,211 | 287,489/ 4,790,582 | 287,489/ 4,790,582 | 287,489/ 4,790,582 | 287,489/ 4,790,582 |
| Rock Type | Basaltic Andesite | Andesite | Basaltic Andesite | Basalt | Basaltic Andesite | Gabbro | Basaltic andesite |
| **Major elements (wt%)** | | | | | | | |
| $SiO_2$ | 54.60 | 57.65 | 53.00 | 46.70 | 55.50 | 42.00 | 52.70 |
| $TiO_2$ | 1.21 | 0.93 | 1.19 | 1.56 | 0.82 | 1.55 | 1.09 |
| $Al_2O_3$ | 18.30 | 18.20 | 16.50 | 17.60 | 19.00 | 18.90 | 17.95 |
| $Fe_2O_{3\_total}$ | 8.20 | 6.45 | 9.20 | 11.35 | 6.95 | 13.63 | 8.46 |
| MnO | 0.14 | 0.15 | 0.17 | 0.17 | 0.21 | 0.23 | 0.21 |
| MgO | 2.88 | 1.90 | 4.53 | 5.30 | 2.33 | 5.45 | 3.48 |
| CaO | 7.86 | 6.44 | 9.76 | 12.30 | 8.40 | 14.20 | 8.77 |
| $Na_2O$ | 3.15 | 3.41 | 2.77 | 2.35 | 3.68 | 1.95 | 3.56 |
| $K_2O$ | 2.17 | 3.19 | 1.98 | 1.18 | 1.74 | 0.49 | 1.92 |
| $P_2O_5$ | 0.44 | 0.36 | 0.31 | 0.34 | 0.42 | 0.84 | 0.37 |
| L.O.I. | 1.06 | 1.30 | 0.78 | 1.26 | 0.75 | 0.47 | 1.10 |
| TOTAL | 100.01 | 99.98 | 100.19 | 100.11 | 99.80 | 99.71 | 99.61 |
| **Trace elements (ppm)** | | | | | | | |
| Rb | 43.1 | 83.7 | 57.0 | 28.4 | 38.3 | 4.1 | 46.0 |
| Sr | 1048.3 | 750.0 | 705.0 | 597.4 | 955.6 | 915.7 | 865.0 |
| Ba | 389.3 | 585.8 | 445.0 | 206.2 | 534.3 | 143.4 | 525.0 |
| Sc | 17.0 | 8.5 | 31.0 | 44.0 | 10.0 | 26.0 | 18.0 |
| V | 222.0 | 150.0 | 298.0 | 406.0 | 138.0 | 362.0 | 246.0 |
| Cr | 25.0 | 3.0 | 85.0 | 89.0 | 8.0 | 29.0 | 20.0 |
| Co | 18.0 | 10.0 | 26.0 | 35.0 | 11.0 | 26.0 | 20.0 |
| Ni | 8.5 | 1.5 | 18.0 | 19.0 | 4.5 | 13.0 | 13.0 |
| Y | 23.0 | 25.0 | 23.0 | 18.9 | 23.3 | 21.4 | 26.0 |
| Zr | 147.0 | 172.0 | 130.0 | 85.0 | 134.0 | 50.0 | 148.0 |
| Nb | 9.8 | 10.4 | 8.1 | 5.9 | 12.8 | 4.2 | 11.2 |
| Cu | 28.6 | 10.4 | - | 70.4 | 16.7 | 29.9 | - |
| Zn | 85.7 | 94.0 | - | 75.5 | 101.6 | 116.6 | - |
| Ga | 22.0 | 22.0 | - | 18.6 | 24.2 | 23.7 | - |
| Ge | 1.5 | 1.6 | - | 1.7 | 1.7 | 1.5 | - |
| As | 0.8 | 1.5 | - | 2.2 | 1.3 | 0.5 | - |
| Mo | 0.8 | 1.1 | - | 0.8 | 0.9 | 0.2 | - |
| Cd | 0.1 | 0.1 | - | 0.0 | 0.1 | 0.1 | - |
| Sn | 1.3 | 1.5 | - | 1.0 | 1.0 | 1.0 | - |
| Cs | 2.5 | 2.9 | - | 0.9 | 0.8 | 0.1 | - |
| La | 23.8 | 29.2 | 22.5 | 11.8 | 33.9 | 13.2 | 33.0 |
| Ce | 51.3 | 60.6 | 48.0 | 27.8 | 69.3 | 32.8 | 64.0 |
| Pr | 6.9 | 7.5 | - | 4.0 | 8.7 | 5.1 | - |
| Nd | 29.2 | 30.2 | 26.5 | 18.2 | 35.5 | 25.1 | 32.0 |
| Sm | 6.2 | 6.3 | 5.8 | 4.3 | 6.7 | 6.2 | 6.5 |
| Eu | 1.7 | 1.7 | 1.6 | 1.4 | 2.0 | 1.8 | 1.9 |
| Gd | 5.2 | 5.1 | 5.1 | 4.1 | 5.3 | 5.4 | 5.4 |
| Tb | 0.7 | 0.7 | - | 0.6 | 0.7 | 0.8 | - |
| Dy | 4.0 | 4.4 | 4.1 | 3.7 | 4.2 | 4.4 | 4.6 |
| Ho | 0.8 | 0.9 | - | 0.7 | 0.8 | 0.8 | - |
| Er | 2.3 | 2.6 | 2.3 | 2.0 | 2.4 | 2.2 | 2.5 |
| Tm | 0.3 | 0.4 | - | 0.3 | 0.3 | 0.3 | - |
| Yb | 2.0 | 2.4 | 2.2 | 1.7 | 2.1 | 1.7 | 2.4 |
| Lu | 0.3 | 0.4 | - | 0.3 | 0.3 | 0.2 | - |
| Hf | 3.7 | 4.5 | - | 2.2 | 3.4 | 1.7 | - |
| Ta | 0.5 | 0.7 | - | 0.3 | 0.7 | 0.2 | - |
| Pb | 6.0 | 8.5 | - | 2.0 | 5.0 | 1.9 | - |
| Tl | 0.1 | 0.4 | - | 0.1 | 0.2 | 0.0 | - |
| Th | 4.1 | 8.9 | 6.0 | 1.8 | 6.2 | 1.2 | 6.8 |
| U | 1.0 | 2.1 | - | 0.5 | 1.0 | 0.3 | - |

* samples analyzed only by ICP-AES at UBO, Brest (France).
Sc, V, Cr, Co, Ni, Zr analyzed by ICP-AES

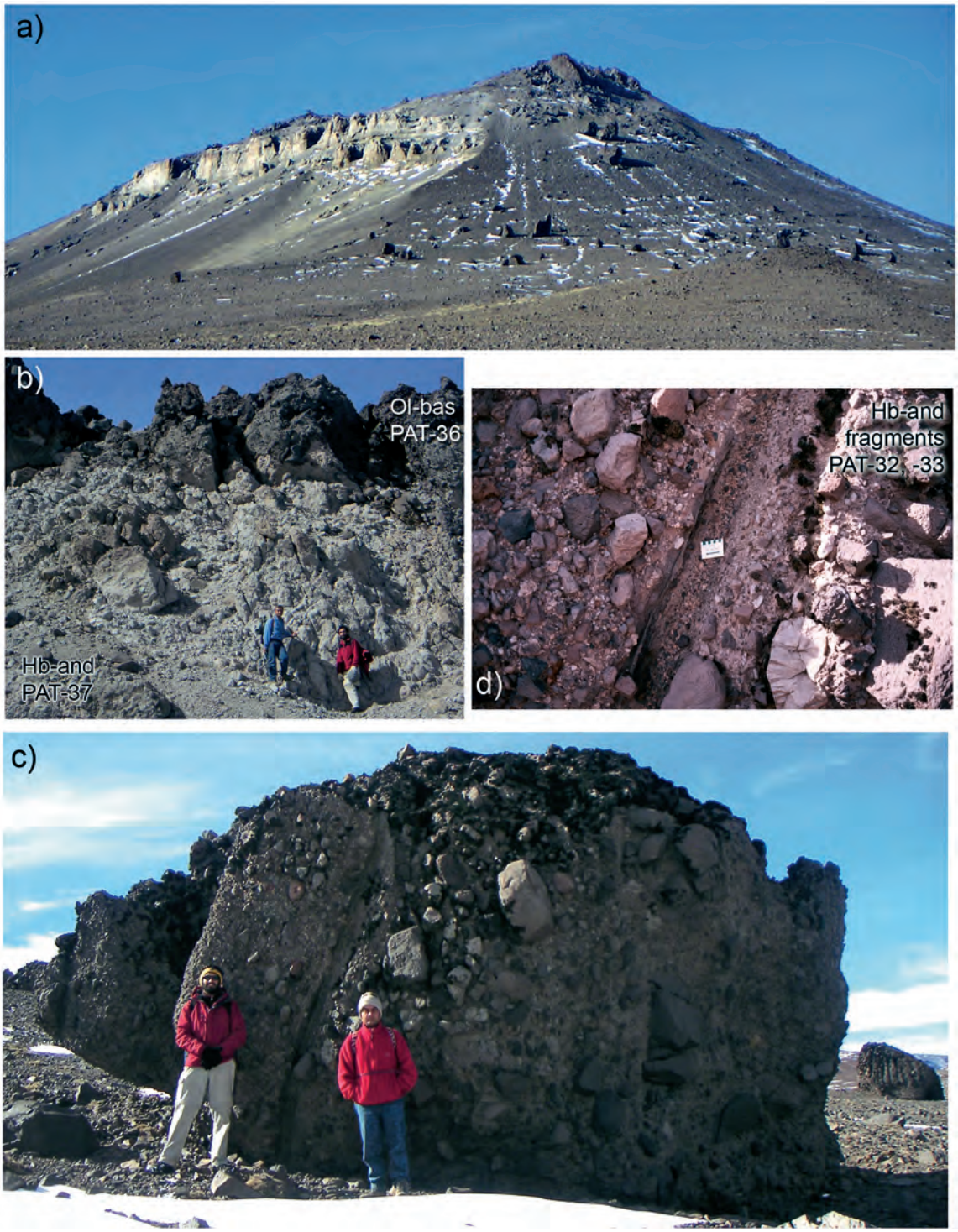


FIG. 3. Field photographs of **a.** view of Cerro Zeballos from the southwest, note the cliff in the upper part formed by the synorogenic sandstones of the Zeballos Group; **b.** part of the studied volcanic sequence outcropping on top of the hill; **c.** large (~4 m diameter) breccia blocks deposited on the south slope of the Zeballos hill; **d.** close up view of the fragments forming the breccia in c (centimetric scale bar in the photograph).

at the LMTG (Toulouse, France). Sr and Nd were first separated from the matrix using the Sr SPEC, LN-SPEC and TRU-SPEC resins, following the technique set up by Pin *et al.* (1995). Sr was loaded on a W single filament with a TaCl 'activator' and Nd was loaded on one of two Re filaments. Isotopic ratios were corrected for any laboratory bias, as described in Benoit *et al.* (1996), using the NBS standard solution for Sr and the La Jolla standard for Nd. The present-day Chondritic Uniform Reservoir (CHUR) value used is 0.512638 for $^{143}Nd/^{144}Nd$.

## 4. Geochronology

The ages of four samples are presented in table 1. They range from uppermost Lower Miocene (16.52 Ma) to Middle Miocene (15.08, 14.82, 14.48 Ma). According to them, the final event of effusive calc-alkaline andesitic volcanism occurred in the Zeballos area at *ca.* 14 Ma, two My after the cessation of plutonism in the NPB and two My before the start of basaltic flood volcanism in the back-arc. These ages agree with those obtained by Boutonnet *et al.* (2010) in similar rocks, and by Marshall *et al.* (1986), Feagle *et al.* (1995) and Blisniuk *et al.* (2005) on tuffs interbedded with sediments of the Santa Cruz Formation (22-14 Ma; Fig. 2b), and with the age of several subvolcanic rocks occurring east of the Patagonian Fold and Thrust Belt in the extra Andean zone (Cerro Indio and Cerro Negro del Ghío: 18-13 Ma, Ramos, 2002; Cerro Moyano: 16±1 Ma, Linares and González, 1990; Table 1). These results indicate that deposition of synorogenic sediments (*i.e.,* the construction of the Patagonian Cordillera) was coeval with a volcanic episode, with a later generation of gravitational debris flows probably resulting from surface uplift. In addition, the existence far south of some coeval intrusives indicates that this Early-Middle Miocene magmatic episode developed all along the extra Andean zone (Michael, 1983; Sánchez *et al.*, 2006).

The age of the youngest dated calc-alkaline sample (14.48 0.36 Ma) suggests a *ca.* 2 Ma quiescence of volcanic activity in the area until the beginning of the basaltic OIB-type volcanism in the Neogene Patagonian Plateau Lavas (12.4 0.4 Ma, Gorring *et al.*, 1997), and especially in the adjacent MLBA (12.18 0.34 Ma, Guivel *et al.*, 2006).

## 5. Mineral chemistry

### 5.1. Lavas

The studied rocks present typical porphyritic to trachytic textures with olivine phenocrysts (in the case of the basalt), pyroxene, amphibole and feldspar, plus Fe-Ti oxides set in a fine grained crystalline groundmass made up of plagioclase laths plus granular to prismatic crystals of clinopyroxene and opaque oxides. Representative electron micropobe analyses of minerals are summarized in table 2.

The basalt (PAT-36) is highly porphyritic; it consists of almost completely altered (iddingsite) subhedral olivine ($Fo_{45-68}$) with Fe-rich rims (Fig. 4c), big (>1 mm) subhedral to euhedral oscillatory-zoned diopside ($Wo_{50-46}En_{43-34}Fs_{8-20}$) and zoned calcic plagioclase phenocrysts ($An_{85-37}Ab_{14-55}Or_{1-8}$). The plagioclase show sieve textures, and are characterized by mineral- and fluid- inclusion rich zones alternating with clean ones. The intergranular groundmass of this sample is

**TABLE 4. Sr-Nd ISOTOPIC DATA FOR MIOCENE CALC-ALKALINE ROCKS OF THE ZEBALLOS VOLCANIC SEQUENCE.**

| Sample | Rock type | Rb | Sr | Sm | Nd | $^{87}Rb/^{86}Sr$ | $^{87}Sr/^{86}Sr$ | $(^{87}Sr/^{86}Sr)o$ | $^{147}Sm/^{144}Nd$ | $^{143}Nd/^{144}Nd$ | $(^{143}Nd/^{144}Nd)o$ | εNd-CHURt |
|---|---|---|---|---|---|---|---|---|---|---|---|---|
| PAT-26 | Basaltic Andesite | 43.1 | 1048.3 | 6.2 | 29.2 | 0.11892 | 0.70366 | 0.70366 | 0.128438 | 0.512780 | 0.512776 | +2.8 |
| PAT-32 | Andesite | 83.7 | 750.0 | 6.3 | 30.2 | 0.32280 | 0.70407 | 0.70400 | 0.126188 | 0.512636 | 0.512624 | +0.1 |
| PAT-36 | Basalt | 28.4 | 597.4 | 4.3 | 18.2 | 0.13751 | 0.70372 | 0.70369 | 0.142916 | 0.512829 | 0.512815 | +3.8 |
| PAT-37 | Basaltic Andesite | 38.3 | 955.6 | 6.7 | 35.5 | 0.11593 | 0.70404 | 0.70402 | 0.114164 | 0.512738 | 0.512727 | +2.1 |
| PAT-38 | Gabbro | 4.1 | 915.7 | 6.2 | 25.1 | 0.01295 | 0.70382 | 0.70382 | 0.149418 | 0.512749 | 0.512749 | +2.2 |
| NBS 987 | Standard | - | - | - | - | - | 0.710238 | - | - | 0.710250 | - | - |
| La Jolla | Standard | - | - | - | - | - | 0.511847 | - | - | 0.511858 | - | - |

made up of tiny Ca-poor plagioclase, diopside prisms and abundant Fe-Ti oxides, with compositions similar to those of the phenocrysts (Fig. 4a, b).

Basaltic andesites (PAT-26, -33, -37, -38A, -39) and a single andesite sample (PAT-32) are porphyritic and rather homogeneous. They contain variable amounts of subhedral zoned Ca-amphibole phenocrysts with compositions varying between edenite, pargasite, hastingsite and hornblende. Calcic to slightly sodic plagioclase ($An_{94-33}Ab_{6-64}Or_{0-3}$) with complex oscillatory zoning patterns is an abundant primary phase (Fig. 4a). Weakly normally zoned augite and diopside ($Wo_{49-46}En_{42-34}Fs_{9-20}$), unzoned clinoenstatite ($En_{67}Wo_4Fs_{29}$) plus Fe-Ti oxides complete the phenocryst assemblage. Groundmasses are fine-grained and made up of plagioclase laths, acicular clinopyroxene plus tiny granular opaque Fe-Ti oxides with compositions similar to those of the phenocrysts (Fig. 4 a, b). In some samples, altered olivine microphenocrysts were also found (Fig. 5d).

### 5.2. Mafic nodules

Mafic nodules show sharp contacts with the host lavas (Fig. 5a). They are holocrystalline coarse-grained amphibole gabbros (Fig. 5b, c), composed by ferroan pargasite- ferroan pargasitic hornblende (45 modal %), anorthite-bytownite plagioclase ($An_{93-84}Ab_{7-16}$, 35 modal %; Fig. 4a), diopside ($Wo_{47-49}En_{38-33}Fs_{15-18}$, 10 modal %; Fig. 4b) partly replaced by amphibole (Fig. 5c), Fe-Ti oxides (5 modal %), and up to 5 modal % accessory apatite and zircon. Mineral intergrowths are common among these crystals. Amphibole and clinopyroxene have compositions similar to those of the host andesite, while plagioclases are Ca-richer in the nodule (Fig. 4).

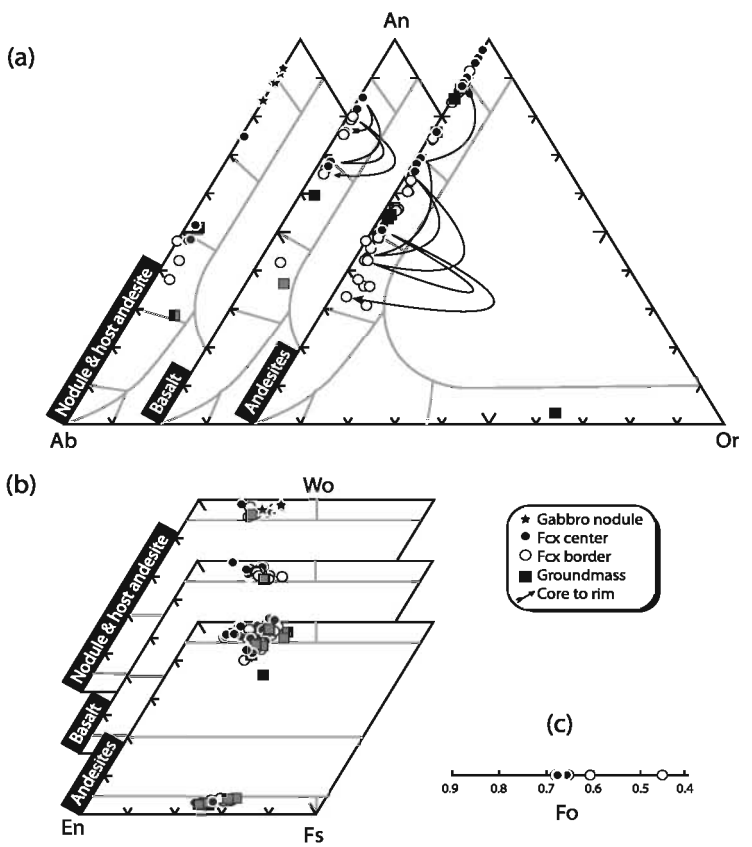


FIG. 4. **a.** Ab-An-Or ternary compositional diagram for analyzed feldspar, **b.** classification diagram for pyroxenes (Morimoto *et al.*, 1988) in the studied rocks; **c.** Forsterite percentage content of olivine in the analyzed basalt. Compositional patterns of oscillatory zonation in plagioclase are indicated by arrows.

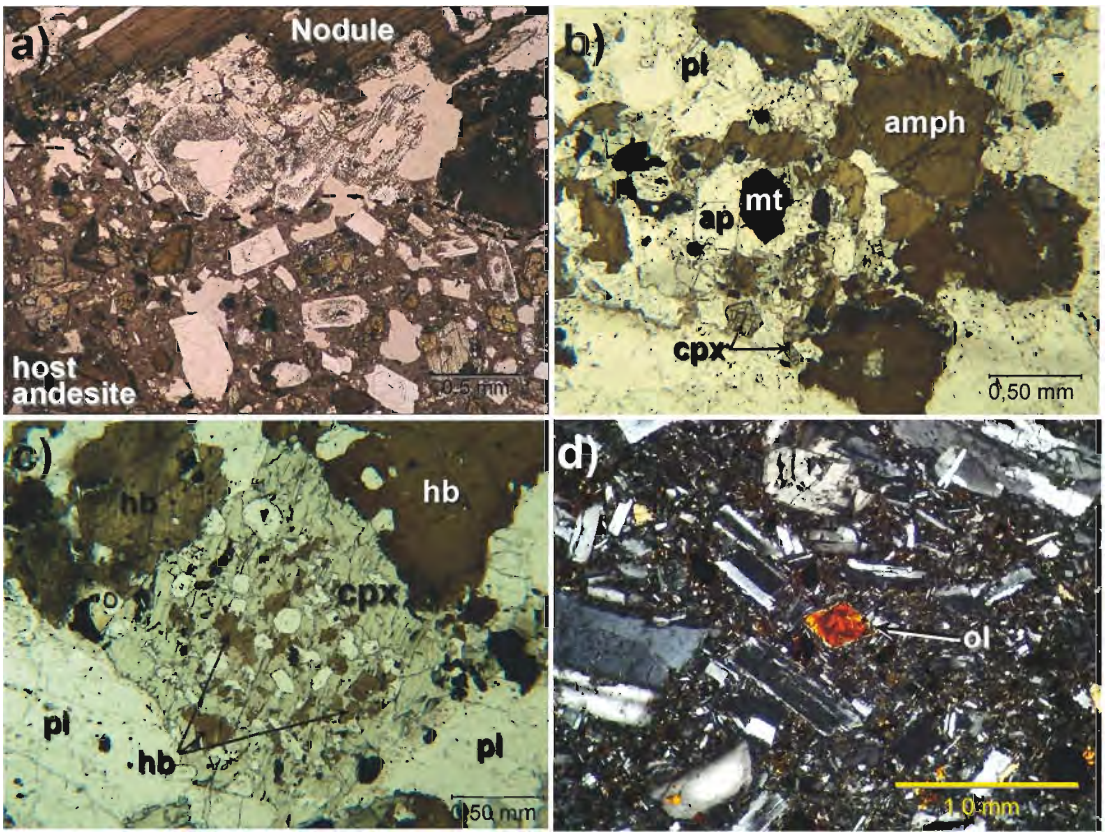


FIG. 5. Microphotographs of rocks from the Zeballos Volcanic Sequence. **a.** Sharp contact between a gabbroic nodule and the host porphyritic lava (dashed line); **b.** mineral assemblage of the nodules (pl+amph+cpx+mt+ap+zr); **c.** Subsolidus disequilibrium texture of clinopyroxenes partially transformed into amphibole in a nodule; **d.** altered olivine microxenocrysts in an Hb-bearing andesite evidencing mixing with basaltic melts (see text for explanations). Scale bar in photographs.

## 6. Geochemistry

### 6.1. Major and trace elements

Samples are subalkaline (according to Irvine and Baragar, 1971) and define a high-K calc-alkaline trend evolving from basalt to basaltic andesites and andesites, in the $SiO_2$ *versus* $K_2O$ diagram (Le Bas *et al.*, 1986; Fig. 6; Table 3). High $Al_2O_3$ and low $TiO_2$ also indicate an arc-like signature for the Zeballos Volcanic Sequence. CIPW norm indicates silica oversaturation (qz-normative) for the intermediate samples, whereas the basalt and the gabbroic nodule are ne-normative. Silica contents vary between 46.7 to 57.7 wt%, and the nodule displays a picritic basalt chemical composition (42 wt% $SiO_2$); the magnesium numbers (mg#) range from 0.52 to 0.40.

Major oxides *versus* silica plots are presented in figure 7a. CaO, $TiO_2$, $Fe_{total}$ and MgO decrease with increasing silica contents, while $K_2O$, $Na_2O$ and $Al_2O_3$ contents tend to increase. The gabbro nodule plots always consistently at the low silica end of each trend defined by the other samples.

Variation diagrams for trace elements (ppm) *versus* silica (wt%) are shown in figure 7b. Highly incompatible elements such as Nb (Fig. 7b) and Zr, Th, Ta, Hf, Th (not shown) display positive correlations with $SiO_2$; while Ni, Cr, Sc (Fig. 7b) and V, Co (not shown) decrease drastically as silica increases. In particular, the Cr contents of the two least differentiated samples (PAT-36 and -33; 89 and 85 ppm Cr, respectively) are significantly higher than those of the other analyzed rocks (3-29 ppm Cr), being similar to those of the Patagonian adakites (81-102 ppm) but lower than the contents of some

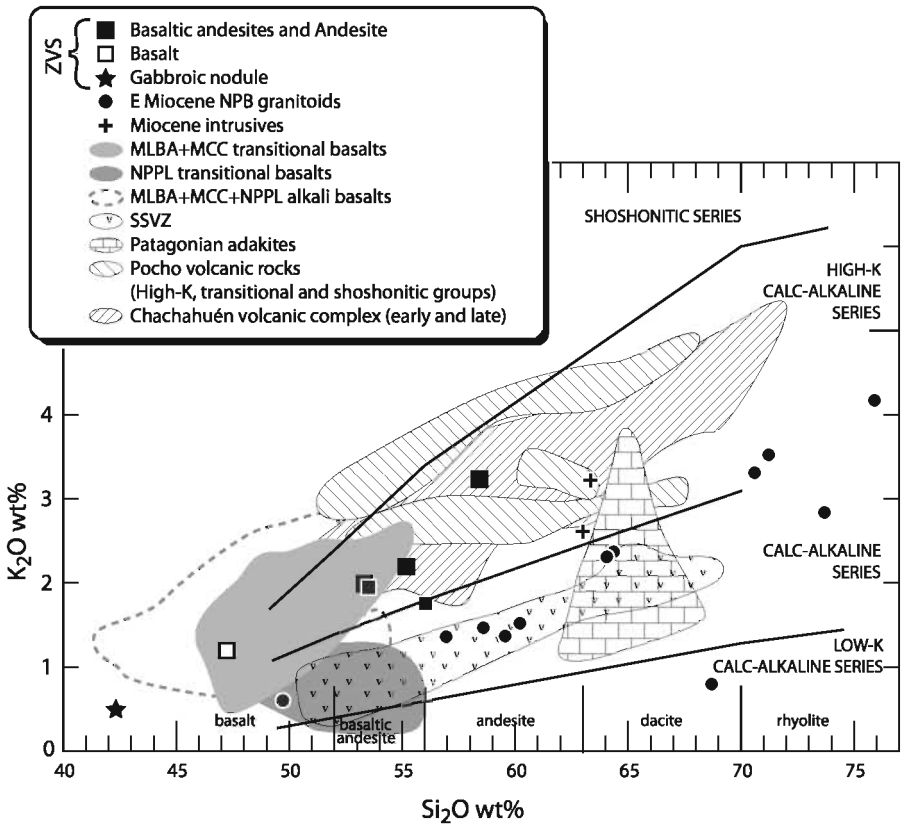


FIG. 6. $SiO_2$ *versus* $K_2O$ wt% diagram (after Peccerillo and Taylor, 1976) for the studied rocks of the Zeballos Volcanic Sequence (ZVS). Miocene andesitic intrusives (black crosses; Ramos *et al.*, 2004) and Lower Miocene North Patagonian Batholith (NPB) granitoids (black circles, Pankhurst *et al.*, 1999; Parada *et al.*, 2000) are also plotted. Fields for Meseta del Lago Buenos Aires (MLBA), Meseta Chile Chico (MCC), main-plateau transitional basalts from the Neogene Patagonian Plateau Lavas (NPPL, 12-4 Ma; Gorring *et al.*, 1997; Gorring *et al.*, 2003; Espinoza *et al.*, 2005; Guivel *et al.*, 2006), Patagonian Adakites (Kay *et al.*, 1993; Ramos *et al.*, 2004), Southern South Volcanic Zone (SSVZ; D'Orazio *et al.*, 2003; López-Escobar *et al.*, 1993; Futa and Stern, 1988) and some South America Flat Slab region volcanic rocks (Pocho volcanic rocks, Kay and Gordillo, 1994; Chachahuén volcanic complex, Kay *et al.*, 2006) were drawn for comparison.

mafic Miocene granitoids of the NPB (213-340 ppm). The same behavior is observed to a lesser extent for Ni and Co. Ba and Sr increase together with silica in the whole series, while Rb content decreases. The most evolved andesitic sample (PAT-32) displays a very high Rb content (84 ppm) compared to the other samples (28-57 ppm Rb; Fig. 7b). Particularly, the Sr content is higher in the studied lavas than in the other calc-alkaline Miocene rocks at similar Si contents, but lower than in the Patagonian adakites (Fig. 7b). The gabbro nodule has higher Sr and Y and lower Sc, Ni, Cr (Fig. 7b) and V, Co (not shown) than the basaltic sample.

Rare Earth Elements (REE) patterns of analyzed samples are presented in figure 8a. Basaltic andesites and the andesite PAT-32 have similar sub-parallel fractionated patterns, enriched in light REE ($(La/Yb)_N$=6.8-10.8) with subhorizontal heavy REE ($(Ho/Yb)_N$=1.2-1.3) and slightly concave downward middle REE patterns ($(Dy/Yb)_N$=1.2-1.3), respectively. No marked Eu anomaly is observed in these rocks. The basalt displays lower REE concentrations than the intermediate samples, with a less fractionated pattern ($(La/Yb)_N$=4.5), no Eu anomaly, no middle REE concavity and slightly more fractionated heavy REE ($(Ho/Yb)_N$= 1.4). The gabbroic nodule pattern has a shape similar to that of the basalt ($(Ho/Yb)_N$=1.5), but displays slightly higher middle to light REE concentrations. As a whole, the REE patterns of the ZVS plot within the field defined by the transitional basalts of the MCC and MLBA plateaus (Fig. 8a).

Primitive mantle-normalized diagrams show that the studied rocks are variably enriched in Large Ion Lithophile Elements (LILE) and homogeneously depleted in High Field Strength Elements (HFSE) (Fig. 8b). Marked negative Nb-Ta, Hf, Ti and positive K, Pb and Sr anomalies are observed for all samples. The analyzed basalt displays lower contents in all incompatible trace elements than the intermediate lavas. The gabbroic nodule is extremely depleted in the most incompatible elements, and displays marked negative Rb, Nb-Ta, Hf-Zr and positive P anomalies. Once again, the studied rocks plot consistently within the field defined by the transitional basalts of MCC and MLBA, which are characterized by similar anomalies (Espinoza *et al.*, 2005; Guivel *et al.*, 2006).

### 6.2. Sr-Nd isotopes

Four lava samples (a basalt, two basaltic andesites and an andesite) and the gabbroic nodule were analyzed for Sr and Nd isotopic compositions (Table 4). The corresponding data, after age corrections, form a coherent trend in the second quadrant of the Sr-Nd diagram (Fig. 9). The initial $^{87}Sr/^{86}Sr$ of the five samples is restricted to values ranging between 0.70366-0.70402, and all but the andesite (the most evolved analyzed lava) display a narrow range of $\varepsilon_{Nd}$ values between +2.1 and +3.8, while the andesite has a lower $\varepsilon_{Nd}$ (+0.1). The analyzed rocks plot close to the Early Miocene NPB granitoids (Pankhurst *et al.*, 1999), but differ significantly from Mesozoic intrusives and Late Miocene-Pliocene satellite bodies of the Batholith, which have a more radiogenic signature. In addition, the ZVS rocks plot within the field defined by the transitional basalts (~12-4 Ma) of the Neogene Patagonian plateau lavas (Gorring *et al.*, 1997; Gorring and Kay, 2001; Espinoza *et al.*, 2005; Guivel *et al.*, 2006).

## 7. Discussion

### 7.1. Evidence of evolution by fractional crystallization for the Zeballos Volcanic Sequence

Major and trace element variation diagrams suggest derivation by fractional crystallization of the Zeballos Volcanic Sequence from a parental basaltic liquid, similar in composition with basalt PAT-36. The compatible behavior of some major and trace elements such as CaO, $TiO_2$, $Fe_{total}$, MgO and Sc, Ni, Cr and V, Co suggests early olivine and later clinopyroxene plus Fe-Ti oxide fractionation from this kind of magma. In addition, amphibole fractionation is suggested by the decrease of Rb/Ba, K/Ba and Dy/Yb ratios (concave-downwards middle REE patterns of the intermediate lavas, with $(Dy/Yb)_N$=1.2-1.3), although apatite fractionation may also contribute to this feature. The rather regular increase of $Na_2O$ and $Al_2O_3$ with silica contents of the lava samples, along with its fairly high Sr concentrations and the lack of significant Eu anomalies, suggest that plagioclase fractionation did not control the differentiation process at any stage. Similarly, alkali feldspar fractionation is not recorded in ZVS rocks chemistry, as indicated by the increase of Ba with silica contents. Highly incompatible elements as Th, Nb, Ta, Hf, Zr, Y and REEs are enriched in the most differentiated samples, suggesting that these elements were stored in the residual liquid as fractionation of major and accessory phases occurred. Similar characteristics are partially recognized in other Miocene calc-alkaline Patagonian rocks (NPB granitoids and back-arc intrusives; Fig. 7a, b).

Depletions in Rb, Nb-Ta, Hf-Zr and enrichment in P in the gabbro nodule are consistent with crystallization of hornblende, zircon and apatite, which are present in high modal abundances in this rock. Panjasawatwong *et al.* (1995) have shown a strong control of melt CaO and $Al_2O_3$ on the plagioclase An content, concluding that $An_{\sim 90}$ plagioclase cannot crystallize from intermediate magma under any P-T-$H_2O$ conditions. Moreover, this composition can only be produced by crystallization from water-rich basaltic melts. Therefore, the nodules from ZVS lavas record the addition of considerable amounts of water either to the melting zone where calc-alkaline melts were produced or to primitive basaltic liquids (from which mineral phases in the nodules would have crystallized), which would have later interacted with intermediate melts (see below). Moreover, absence of Eu anomalies in the REE patterns of analysed rocks (Fig. 8a) suggest that magmas were stabilized under high pressure and/or oxidizing conditions, further suggesting water involvement (*e.g.*, Aigner-Torres *et al.*, 2007). The application of the Holland and Blundy (1994) geothermometer to several amphibole-plagioclase pairs evidencing equilibrium (as inclusions or in direct contact) yields crystallization temperatures between 980° and 880°C for pressures of 1 and 0.5 GPa, respectively.

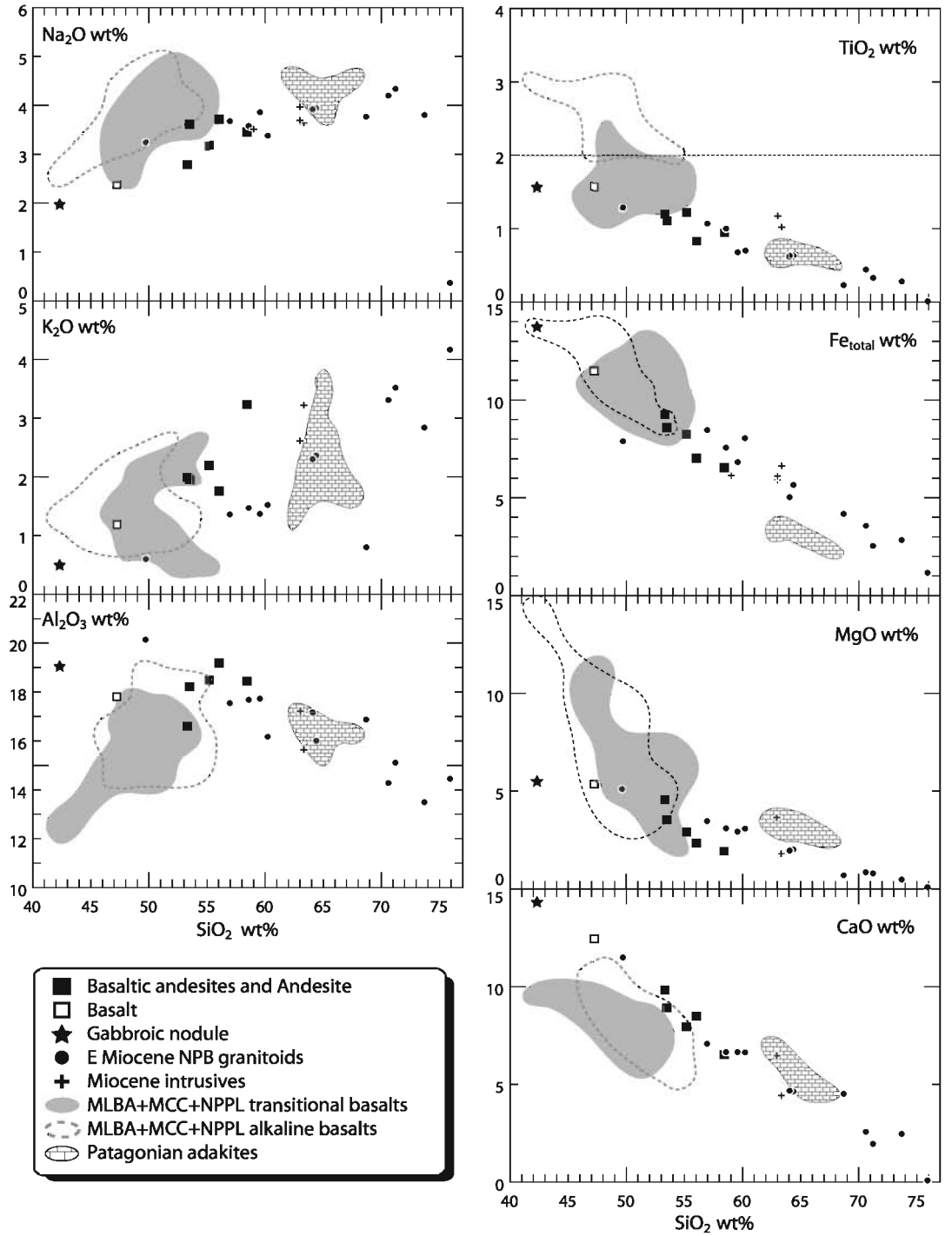


FIG. 7a. Selected major oxides (wt%, values on anhydrous basis) *versus* silica (wt%) diagrams for rocks of the Zeballos Volcanic Sequence. Lower Miocene North Patagonian Batholith (NPB) granitoids (Pankhurst *et al.*, 1999; Parada *et al.*, 2000) and Miocene intrusives (Ramos *et al.*, 2004) are also plotted. Compositional fields for Meseta del Lago Buenos Aires (MLBA), Meseta Chile Chico (MCC) and the Neogene Patagonian Plateau Lavas (NPPL) transitional and alkaline basalts (*ca.* 12-4 Ma; Gorring *et al.*, 1997; Espinoza *et al.*, 2005; Guivel *et al.*, 2006) and that for the Patagonian Adakites (Kay *et al.*, 1993; Ramos *et al.*, 2004) were drawn for comparison.

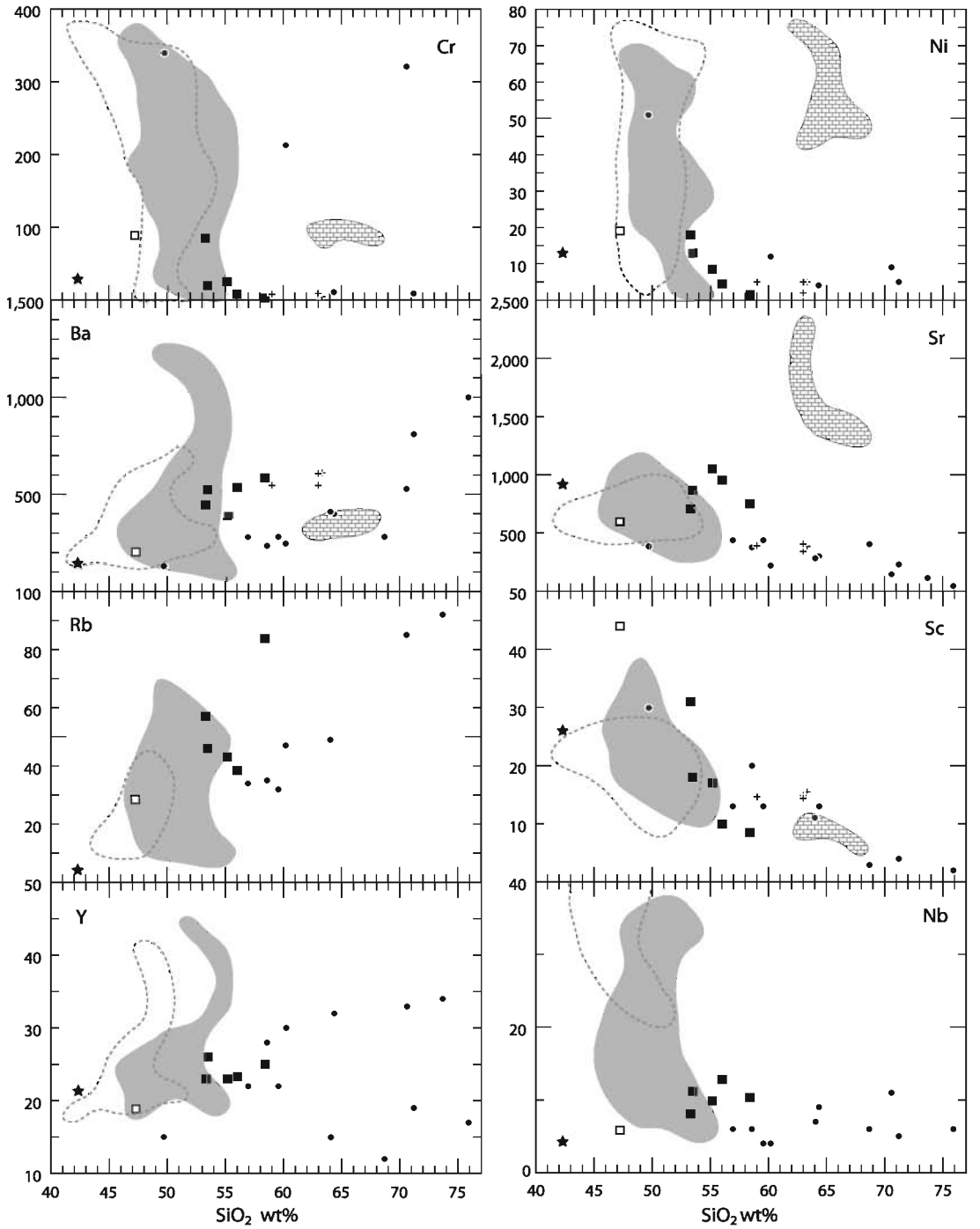


FIG. 7b. Selected trace elements (ppm) *versus* silica (wt%) diagrams for rocks of the Zeballos Volcanic Sequence. Simbology as in figure 7a.

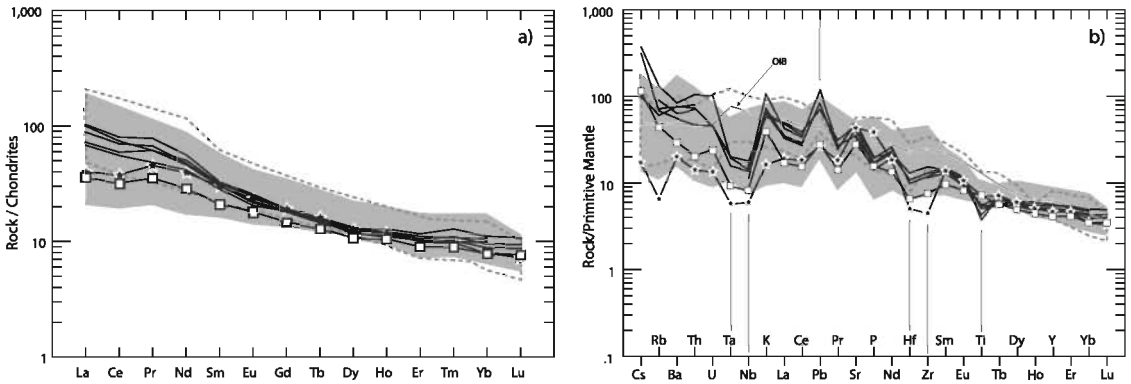


FIG. 8. **a.** Chondrite-normalized (Nakamura *et al.*, 1973) rare earth elements diagrams and **b.** Primitive mantle-normalized (Sun and McDonough, 1989) trace elements for rock samples of the Zeballos Volcanic Sequence. Compositional fields for Meseta del Lago Buenos Aires (MLBA), Meseta Chile Chico (MCC) and the Neogene Patagonian Plateau Lavas (NPPL) transitional (light grey field) and alkaline basalts (segmented line) (*ca.* 12-4 Ma; Gorring *et al.*, 1997; Espinoza *et al.*, 2005; Guivel *et al.*, 2006) were drawn for comparison. OIB patterns from Sun and McDonough (1989). Simbology as in figure 7a.

## 7.2. Possible origin of the transitional signature of some Neogene Patagonian plateau basalts

The transitional signature of Neogene Patagonian Plateau Basalts is defined as an intermediate between alkaline and calc-alkaline geochemical affinities, characterized by arc-like magmatism features (Nb and Ti depletions, La/Nb>1, low Ce/Pb and Nb/U), combined with a clear OIB-type intraplate imprint (Ba/La=10-20, high contents in both LILE and HFSE). The origin of this signature has been attributed to the generation of these plateau basalts from an enriched asthenospheric source combined with the contribution of a lithospheric component involving: **i)** subducted basaltic slab-derived melts/fluids, **ii)** subducted crustal sediment-derived fluids/melts, and/or **iii)** older calc-alkaline magmas (not previously recognized) stored at crustal levels (Gorring and Kay, 2001; Espinoza *et al.*, 2005; Guivel *et al.*, 2006). As shown by Guivel *et al.* (2006), the intensity of Nb and Ti depletion is attenuated during differentiation, suggesting that it is related to the 'local' source of these basalts rather than representing an overall regional mantle feature. Therefore, these anomalies are likely related to the occurrence of a restitic rutile-bearing residue of slab melts (produced at the edges of the slab tear, see Thorkelson and Breitsprecher, 2005; Guivel *et al.*, 2006) in the shallow asthenospheric or deep lithospheric Patagonian mantle. Indeed, rutile retains only Nb, Ta and Ti and is commonly observed as a residual phase during partial melting of oceanic basalts under P-T conditions consistent with those of hot subduction zones (Ringwood, 1990; Foley *et al.*, 2000; Schmidt *et al.*, 2004). In addition, *ca.* 9 Ma old calc-alkaline rhyolitic tuffs interbedded with basalts of MCC were previously thought to be responsible (by mixing processes) for this signature (Espinoza *et al.*, 2005). However, other major and arc-like trace element characteristics observed in the transitional basalts (*e.g.*, slightly higher $SiO_2$, Th/Yb, Zr/Nb and lower Ce/Pb than those of alkali basalts; Fig. 10), are not explained by the process described above. Then, the influence of a subduction component in the chemistry of transitional basalt represented by the ZVS magmas, is supported by arc-like signature recognized in their trace element contents (La/Nb>1, high Th/Nb and Ba/Nb, low Nb/Zr and Ta/Hf<0.4; Fig. 10). Furthermore, trace elements contents and ratios (LILE/HFSE; HFSE/HFSE) of transitional basalts plot consistently between those of genuine alkali basalts and ZVS rocks, suggesting a mixing origin for them (*e.g.*, Ce/Pb, Nb/U, La/Yb, LILE/Nb; Fig. 10). In addition, disequilibrium features evidencing mixing are recognized in plagioclase from the intermediate lavas and the basalt as oscillatory zoning patterns (Fig. 4a), and in some basaltic andesites where altered olivine microphenocrystals are found (Fig. 5d). Further evidence supporting the mixing hypothesis is the fact that transitional basalts were emplaced randomly during the main-plateau volcanic stage (Guivel *et al.*, 2006), and their flows are interbedded with those of pure alkali basaltic composition.

### 7.3. Miocene calc-alkaline magma sources

The calc-alkaline nature of ZVS rocks suggests that these magmas would have been generated by some type of subduction-related magmatic processes, as reflected by its chemical signature. Then, magma source of ZVS could have been variably influenced by subducting slab and/or subducted sediments fluids/melts and/or continental crust material, as usually envisioned for subduction-related magmatism (*e.g.*, Ellam and Hawkesworth, 1988). However, a clear crustal signal is not recognized in ZVS magmas neither in their trace elements features nor in their isotopic ratios (see Figs. 7, 9). Rather low contents of source enrichment tracers (*e.g.*, Ta, Hf, Nb) and unradiogenic isotopic ratios are consistent with derivation of the ZVS magmas from an incompatible element-depleted and unradiogenic mantle source. Besides, flat HREE patterns ($(La/Yb)_N$=10-15; $(Sm/Yb)_N$=2.5-3.5; Fig. 10e) preclude their derivation from a deep garnet-bearing source similar to that of NPPL basalts (Gorring *et al.*, 1997; Gorring and Kay, 2001; Espinoza *et al.*, 2005). On the other hand, subducted sediments fluids/melts involvement could be depicted by Th contents (*e.g.*, Kilian and Behrman, 2003). Th is often metasomatically added to arc mantle-source regions, a process which leads to accentuate the negative Nb anomalies characteristic of arc magmas in multielemental spider diagrams (*e.g.*, Fig. 8b). In the Nb/Yb *versus* Th/Yb diagram of Pearce and Peate (1995) (Fig. 10a), ZVS rocks plot towards higher Th at a given Nb than do NPPL alkali basalts, which lie well within the mantle array (consistent for rocks with very little or lacking subduction components), reflecting an arc-type sediment imprint in the source of studied rocks. Furthermore, fluid-mobile element signature varies with differentiation (increasing LILE/HFSE: Th/Nb,

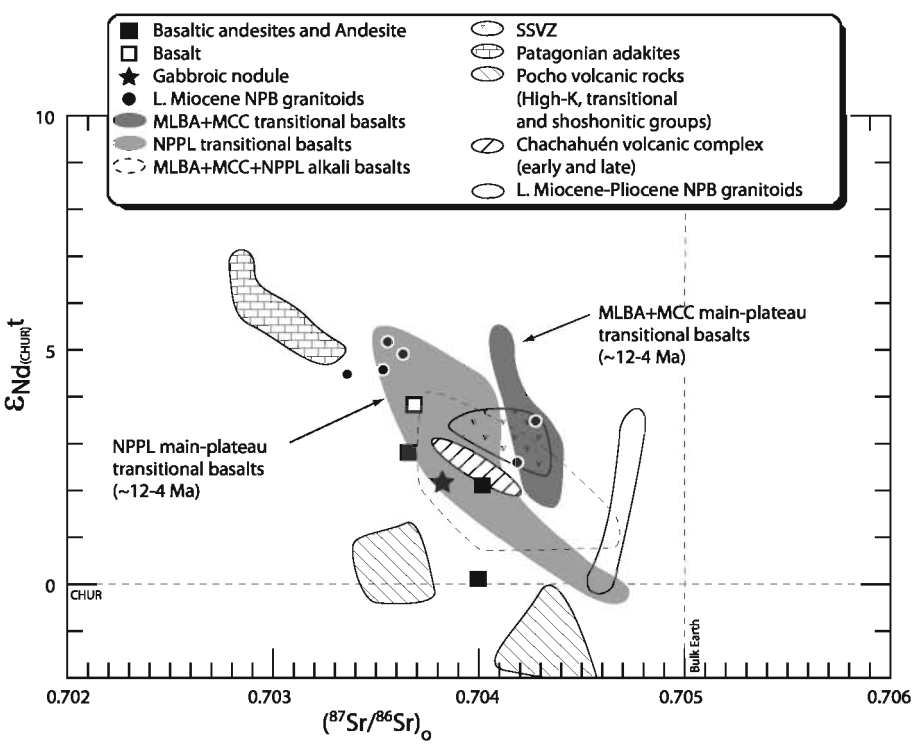


FIG. 9. $(^{87}Sr/^{86}Sr)_o$ *versus* $\varepsilon_{Nd}$ diagram for rocks of the Zeballos Volcanic Sequence. Lower Miocene granitoids of the North Patagonian Batholith (NPB, Pankhurst *et al.*, 1999) are also plotted. Fields for Upper Miocene-Pliocene granitoids of the NPB (Pankhurst *et al.*, 1999), Meseta del Lago Buenos Aires (MLBA), Meseta Chile Chico (MCC) and the Neogene Patagonian Plateau Lavas (NPPL) main-plateau basalts (transitional and alkaline) (Gorring *et al.*, 1997; Espinoza *et al.*, 2005; Guivel *et al.*, 2006), Southern South Volcanic Zone (SSVZ; D'Orazio *et al.*, 2003; López-Escobar *et al.*, 1993; Futa and Stern, 1988), Patagonian adakites (Kay *et al.*, 1993; Ramos *et al.*, 2004), Pocho (Kay and Gordillo, 1994) and Chachahuén volcanic rocks (Kay *et al.*, 2006) were drawn for comparison. Isotopic values recalculated at 15 Ma. See text for discussion.

Th/Hf, Ba/Nb, decreasing Ce/Pb; Fig. 10c, d, g), implying that the influence of subducted sediment components varied throughout magmatic evolution. In addition, the higher than-MORB Th/U ratio of ZVS rocks confirms the need for sediment addition to its mantle source.

Regarding Miocene magma sources, the lack of any important crustal signature both in the former westernmost arc (NPB) and the studied volcanic rocks is noteworthy. Miocene granitoids are mostly mafic rocks with calc-alkaline affinity, directly related to subduction, having primitive isotopic signatures (Fig. 9). Crustal influence (high $^{87}Sr/^{86}Sr$) is only recognized in older (Mesozoic) and younger (Late Miocene-Pliocene) granitoids from the NPB (Pankhurst *et al.*, 1999). Thus, the fairly similar unradiogenic isotopic signatures of Miocene rocks suggest a rather common mantle source (Fig. 9). Coeval and later to ZVS, the Patagonian adakitic rocks have high Cr, Ni and Sr contents, HREE depletion and strongly unradiogenic isotopic signatures. All these features are consistent with melts generated from the subducting slab and then ascending through an enriched mantle wedge, where compatible elements such as Cr and Ni would be included into the uprising liquids (Kay *et al.*, 1993; Ramos *et al.*, 2004). In the ZVS, the two less differentiated rocks have higher Cr contents, and to a minor extent Ni contents, than those of the intermediate lavas, and similar to those of Patagonian adakites and to some NPB granitoids (Fig. 7b). This evidences the interaction of parental ZVS liquids, and similarly, of NPB magmas, with an enriched component, probably represented by the mantle above their melting regions.

As shown previously, ZVS and Miocene intrusives share geochemical features with the Miocene NPB granitoids, but also they differ significantly. First, they belong to a high-K series, while coeval NPB granitoids display a low-K calc-alkaline trend (Fig. 6). Second, although similar behaviors are observed for some major and trace elements, discrepancies in MgO, $Al_2O_3$ and in Sr, Ba, Y, Nb and Th contents between them and NPB granitoids suggests that their magmatic evolution followed different fractionation trends (Fig. 7). La/Yb and Nb/Zr ratios of ZVS lavas (and of the intrusives) are intermediate between the NPPL alkali basalts, the NPB arc granitoids and the active volcanoes from the southern Andes. Since the Nb/Zr ratio of the studied samples does not vary significantly with differentiation nor, for example, with $^{143}Nd/^{144}Nd$ (not shown), it is unlikely to be related with fractionation or contamination processes (*e.g.*, sediment involvement in the source as suggested for some island arcs, *e.g.*, Vroon *et al.*, 1995), then it should trace a primary feature of the ZVS magma source. Therefore, these ratios allow to discriminate the source region enrichments between the earlier arc magmatism (NPB) and a later eastern calc-alkaline volcanism (ZVS), and also to introduce the hypotesis that the ZVS magmatism have similar source characteristics with flat-slab related calc-alkaline rocks of the Central Andes (Pocho and Chachahuén complexes; Kay and Gordillo, 1994; Kay *et al.*, 2006; Figs. 10e, f).

### 7.4. Proposed Model: Transient Middle Miocene shallow subduction related with the Chile Ridge collision

To explain the occurrence of subduction-like magmatism far from former arc regions some geotectonic models have been developed. In the case of Central Chile-Argentina (in the so-called Andean flat-slab region), models involving the shallowing of the subducting Neogene plate since *ca.* 8 Ma and the generation of a secondary dehydration front far away from the arc position have been proposed (Kay and Gordillo, 1994; Kay and Mpodozis, 2002). This phenomena would induce the generation of sub-alkaline magmas by slab dehydration and mantle-wedge processes (*e.g.*, Tatsumi and Eggins, 1995; Grove *et al.*, 2003), resulting in the extrusion of high-K amphibole-bearing basaltic to dacitic magmas with a strong arc-like component near *ca.* 500-700 km east of the present trench and also a tectonic efect. In this case, the phenomenon triggering this process would have been the subduction of the Juan Fernández Ridge hotspot track (Foley *et al.*, 2000; Yáñez *et al.*, 2001). In Ecuador, the abnormal width of the active volcanic arc (~120 km) and the abundance of adakites and magnesian andesites with adakitic affinity have been accounted for by the flat or low-angle subduction of the Pacific plate, linked to the arrival to the trench of the Carnegie Ridge (Gutscher *et al.*, 2000; Beate *et al.*, 2001; Bourdon *et al.*, 2003). In Patagonia, shallow syncollisional subduction was suggested by Gorring *et al.* (1997) in relation with the subduction at *ca.* 15 Ma of the Chile Ridge (Cande and Leslie, 1986) and the

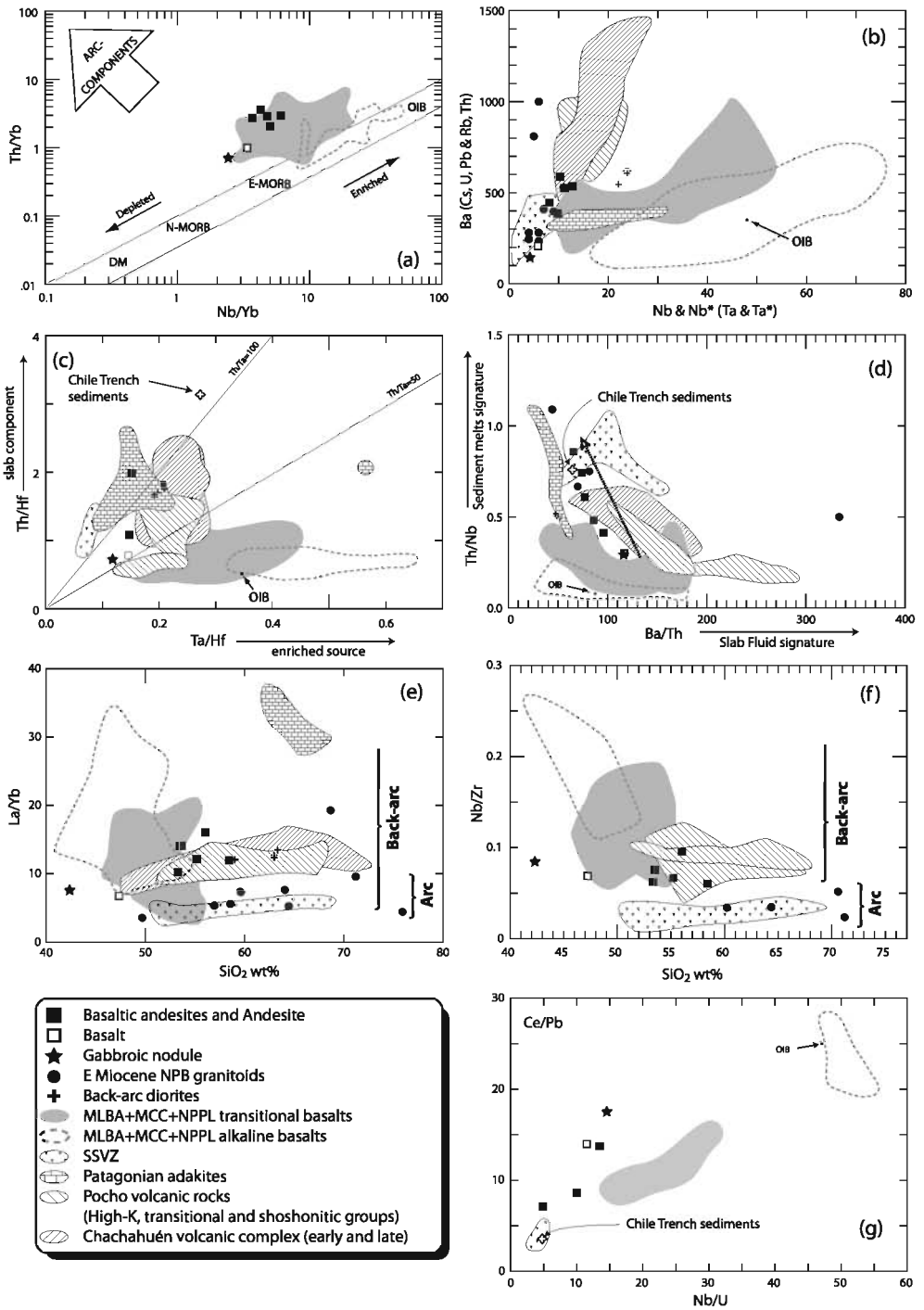


FIG. 10. Trace elements ratio diagrams for rocks of the Zeballos Volcanic Sequence. Lower Miocene North Patagonian Batholith (NPB, Pankhurst *et al.*, 1999; Parada *et al.*, 2000) and Miocene intrusives (Ramos *et al.*, 2004) are also plotted. Other compositional fields as in figure 6. **a.** Th/Yb *versus* Nb/Yb; **b.** Ba (or other LILE or fluid-mobile element) *versus* Nb (or Ta); Nb*=17×Ta (after Sun and McDonough, 1989); **c.** Th/Hf *versus* Ta/Hf; **d.** Th/Nb *versus* Ba/Th; **e.** La/Yb *versus* $SiO_2$ wt%; **f.** Nb/Zr *versus* $SiO_2$ wt%, and **g.** Ce/Pb *versus* Nb/U. Arrow in d) indicates the fractionation trend of the ZVS rocks. Composition of Chile Trench sediments (Kilian and Behrmann, 2003) is indicated in some diagrams. Symbology in the figure. See text for discussion.

opening of a slab window under the continent, and by Suárez *et al.* (2000) regarding timing of deformation in the Patagonian fold and thrust belt, but no further analysis of this process has been carried out. In the next sections we present a model to show the development, during the Middle Miocene, of a transient low-angle subduction beneath Patagonia that provoked the eastward migration of the arc front and the consequent generation and extrusion of calc-alkaline magmas.

#### *7.4.1. Geodynamic constraints: convergence kinematics and ridge subduction*

Changes in the convergence parameters (angle and rate) between the Nazca and South American plates are reported during the Cenozoic. The *ca.* 15 Ma ridge-trench collision at 55°S (Cande and Leslie, 1986) occurred synchronously with one of the two events when subduction parameters changed, during which high convergence rates (from *ca.* 30 mm/yr at 30 Ma up to 110 mm/yr at 15 Ma) and slightly oblique subduction (*ca.* 79°) were registered (Pardo-Casas and Molnar, 1987; Somoza, 1998) (see Fig. 11). As established by Pankhurst *et al.* (1999), these periods coincide with intense plutonic activity in the North Patagonian Batholith, and generated magmas are mostly mafic with unradiogenic isotopic signatures. The subduction of young, hot and buoyant oceanic lithosphere coupled with an increase in the convergence rate would cause a decrease in the slab dip (see Jordan *et al.*, 2001 and references therein). One problem arising from this hypothesis is that it would take many million years to equilibrate the slab (*i.e.*, to reach a low subduction angle) within a resistant-to-flow asthenosphere. For the Neogene Patagonian mantle it has been shown that it has a low density and stayed rather hot since, at least, Eocene times (*e.g.*, Murdie *et al.*, 2000; Heintz *et al.*, 2005; Espinoza *et al.*, 2005). This supports the possibility that the slab could reequilibrate with the asthenosphere not long after kinematics changed and young oceanic lithosphere subducted under Patagonia (as the Chile Ridge approached the continent), supporting the development of transient shallow subduction during the Middle Miocene.

#### *7.4.2. Chemical similitudes with Andean Flat-slab volcanics*

Further support for emplacement of the ZVS and the Miocene diorites over a gently dipping subducting slab comes from their chemical similarities with volcanic rocks of the Pocho volcanic complex (Kay and Gordillo, 1994) in the Chilean flat-slab region (28°-33°S, see Kay and Mpodozis, 2002) and of the Chachahuén volcanic complex (37°S; Kay *et al.*, 2006) in the Neuquén Basin (see Kay and Ramos, 2006). Chemical similarities between the ZVS lavas, the Miocene diorites and these flat-slab magmas include: **i)** high $K_2O$ contents (Fig. 6); **ii)** similar La/Yb, La/Sm and Sm/Yb ratios (Table 3); and **iii)** similar Nb/Zr, La/Nb, Ba/Nb, Th/Hf, Th/Ta, Ta/Hf ratios (Fig. 10). On the other hand, whereas long-term Andean flat-slab volcanism evolved towards a more arc-like signature (*e.g.*, Kay and Gordillo, 1994; Kay *et al.*, 2006), Patagonian magmas evolved temporally towards a more primitive end member (Pliocene 'post plateau' mafic volcanism), perhaps as a result of the transient nature of the proposed Middle Miocene shallow subduction event.

Our chemical data for the ZVS rocks are consistent with the development during Middle Miocene of a transient low-angle subduction under Patagonia (Fig. 11). The particular geodynamic framework in the southeastern Pacific at this time gives a consistent support for this hypothesis. Thermal and age characteristics of the subducting Nazca slab were globally favorable to a decrease in the subduction angle. However, the approach to the trench of the active Chile Ridge seems to be the main factor for triggering the decrease in the subduction angle. As the Chile Ridge approached to the continent and the Farallon (Nazca) Plate becames younger close to the trench, the shallowing of the slab begun and the first calc-alkaline magmas (ZVS) erupted in the MLBA region (*ca.* 16 Ma). The shallowing slab would reach melting temperatures *ca.* 300 km east from the trench and released enough water (mainly from subducted sediments mineral dehydration) to stabilize amphibole (then generating oxidizing conditions). Under these thermal and geodynamic conditions, a new regime for magma genesis would be set. Calc-akaline liquids from this source (incompatible elements-depleted and isotopically unradiogenic) would interact with a primitive component (high Cr and Ni) in the mantle wedge above, modifying the chemistry of parental ZVS magmas. A relatively high degree of melting of this source, either mantle wedge- or lithospheric-like, and later mineral fractionation with negligible involvement of the crust would produce the chemistry of the studied rocks.

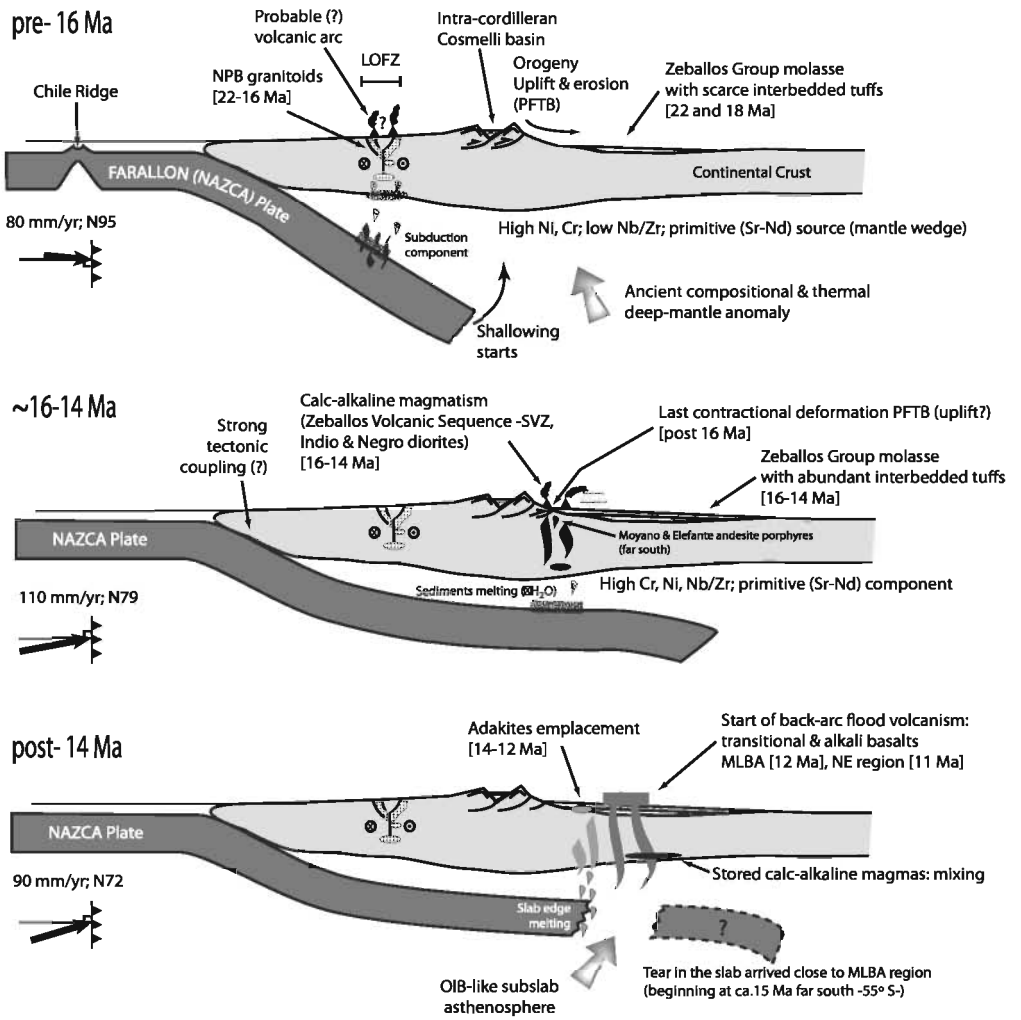


FIG. 11. Schematic cross sections (not to scale) of Patagonian lithosphere during the Early Miocene near the latitude of Meseta del Lago Buenos Aires (MLBA, ~47°S) where petrogenetic and tectonic models supporting the generation of calc-alkaline magmatism in the present-day back-arc domain are presented. Sections include magmatic and tectonic events that occurred at different latitudes between 44° and 55°S. Pre- ~16 Ma: near orthogonal and relatively slow normal-angle subduction; shallowing of the slab begins as the Chile Ridge approaches the trench; mafic calc-alkaline primitive plutonism (in terms of Sr-Nd isotopes) is generated below the arc associated with the Liquiñe-Ofqui Fault Zone (LOFZ) (Lower Miocene granitoids of the North Patagonian Batholith, NPB); deformation and uplift along the Patagonian Fold and Thrust Belt (PFTB); deposition of synorogenic sediments in the foreland together with sporadic explosive volcanism. ~16-14 Ma: changes in the convergence parameters occurred (convergence rate increases and oblique subduction); collision of the Chile Ridge with the trench at *ca.*, 15 Ma far south (~55°S); transient low-angle subduction under Central Patagonia; end of plutonism below the arc; high-K calc-alkaline magmatism in the back-arc domain (ZVS and intrusives); last compressive event in the PFTB. Post ~14 Ma: oblique subduction continues and convergence rate decrease; calc-alkaline magmatism of the ZVS ceased when the tear in the Nazca slab (generated after Chile Ridge collided at 55°S and which propagated northward) arrived below the MLBA region; later, deep sub slab asthenosphere-derived alkaline basaltic melts arose through the tear in the slab and extruded extensively in the back-arc of Patagonia (main-plateau stage); interaction of these melts with stored calc-alkaline magmas (related to the ZVS) produced transitional basalts which were extruded concomitantly with pure alkaline lavas; melts of slab edges extruded as adakitic magmas also in a back-arc position. For each described period, the E-W component of the convergence rate (mm/yr) between the Nazca and South American plates (averaged for periods between major magnetic anomalies) and the convergence angle with respect to the present day North, are indicated by an oriented arrow (from the data of Pardo-Casas and Molnar, 1987 and Pankhurst *et al.*, 1999). LOFZ tectonics inferred from Pliocene transpressional pop-up structure (Cembrano *et al.*, 2002); NE: North East volcanic region in Santa Cruz, Argentina.

The shallowing of subduction angle continued up to *ca.* 14-12 Ma when the tear in the Nazca slab arrived below the MLBA region. Afterwards, alkaline and transitional flood basalts extruded forming the plateau. South of the Lago General Carrera-Buenos Aires area, melts from the subducted Nazca Plate edges were emplaced as adakitic dacites, also in the present-day back-arc domain (Thorkelson and Breitsprecher, 2005; Breitsprecher and Thorkelson, 2009). Finally, Miocene uplift ended at *ca.* 14 Ma after a shortening and compressive phase (Blisniuk *et al.*, 2005; Lagabrielle *et al.*, 2006, 2007), contemporaneously with the end of calc-alkaline magmatism in the MLBA area.

## 8. Conclusions

The Zeballos Volcanic Sequence (ZVS) rocks represent a Middle Miocene high-K calc-alkaline volcanic event in the Patagonian back-arc region.

The evolution of ZVS magmas by fractional crystallization from melts similar to the basalt present in the sequence is supported by major and trace elements; no crustal involvement in this process is recognized.

Amphibole-rich gabbroic nodules included in intermediate lavas are cogenetic implying the addition of considerable amounts of water to the magma source.

ZVS rocks are enriched in LILE and REE and have Nb/Zr, La/Yb, Ce/Pb, Nb/U ratios distinct from those of typical arc-related (Miocene and present) volcanic rocks. These features, as well as high Th, low Th/U and $\varepsilon_{Nd}$ variations, document a strong signature of $H_2O$-rich subducted sediments.

The arc component recognized in the transitional signature of later Mio-Pliocene plateau basalts of the Neogene Patagonian Plateau Lavas (Gorring *et al.*, 1997; Guivel *et al.*, 2006) is thought to have arisen from mixing of alkaline melts with stored calc-alkaline magmas equivalent to those of the ZVS.

Similarities between the ZVS magmas and those from volcanic complexes emplaced above a gently dipping slab (present Andean flat-slab region in Central Chile-Argentina; Late Miocene Neuquén Basin), together with a suitable geodynamic configuration, suggest the occurrence of transient Middle Miocene low-angle subduction in Patagonia, possibly associated with the arrival of the Chile Ridge and the later ridge-trench collision at *ca.* 15 Ma.

## Acknowledgements

This work form part of the first author's PhD thesis (2004-2006 CONICYT-BIRF Chile grant) and part of the ECOS-CONICYT C05U01 (D.M. and Y.L.) and DyETI-INSU-CNRS (Y.L.) projects. The authors would like to thank Dr. P. de Parseval (LMTG, Toulouse, France) for the assistance with the microprobe analyses, Mr. P. Brunet (LMTG, Toulouse, France) for the TIMS measurements and Estancia Sol de Mayo crew (Santa Cruz, Argentina) for the field facilities and hospitality. F.E. thanks to A. Sánchez and F. Gutiérrez for interesting patagonian discussion. Editorial supervision by J. Cembrano and thoughtful and constructive reviews by C.R. Stern, R.J. Pankhurst and S. Jego are greatly acknowledged.

## References

Aigner-Torres, M.; Blundy, J.; Ulmer, P.; Pettke, T. 2007. Laser Ablation ICPMS study of trace element partitioning between plagioclase and basaltic melts: an experimental approach. Contributions to Mineralogy and Petrology 153 (6): 647-667.

Aries, S.; Valladon, M.; Polvé, M.; Dupré, B. 2000. A routine method for oxide and hydroxide interference corrections in ICP-MS chemical analyses of environmental and geological samples. Geostandards Newsletter 24: 19-31.

Beate, B.; Monzier, M.; Spikings, R.; Cotten, J.; Silva, J.; Bourdon, E.; Eissen, J.-P. 2001. Mio-Pliocene adakite generation related to flat subduction in Southern Ecuador: The Quimsacocha volcanic center. Earth and Planetary Science Letters 192: 561-570.

Bell, C.; Suárez, M. 2000. The Río Lácteo Formation of southern Chile. Late Paleozoic orogeny in the Andes of southernmost South America. Journal of South America Earth Sciences 13: 133-145.

Bellon, H.; Quoc Buu, N.; Chaumont, J.; Philippet, J.C. 1981. Implantation ionique d'argon dans une celibe support: application au tracage isotopique d l'argon contenu dans les minéraux et les roches. Comptes Rendus de l'Académie des sciences 292: 977- 980. Paris.

Benoit, M.; Polvé, M.; Ceuleneer, G. 1996. Trace element and isotopic characterization of mafic cumulates in a fossil mantle diapir (Oman ophiolite). Chemical Geology 134: 199-214.

Blisniuk, P.M.; Stern, L.A.; Chamberlain, C.P.; Idleman, B.; Zeitler, P.K. 2005. Climatic and ecologic changes during Miocene surface uplift in the southern Patagonian Andes: Earth and Planetary Science Letters 230: 125-142.

Bourdon, E.; Eissen, J.-P.; Gutscher M.-A.; Monzier, M.; Hall, M.L.; Cotten, J. 2003. Magmatic response to early aseismic ridge subduction: the Ecuadorian margin case (South America). Earth and Planetary Science Letters 205: 123-138.

Boutonnet, E.; Arnaud, N.; Guivel, C.; Lagabrielle, Y.; Scalabrino, B.; Espinoza, F. 2010. Subduction of the South Chile active spreading ridge: A 17 Ma to 3 Ma magmatic record in central Patagonia (western edge of Meseta del Lago Buenos Aires, Argentina). Journal of Volcanology and Geothermal Research 189: 319-339.

Breitsprecher, K.; Thorkelson, D.J. 2009. Neogene kinematic history of Nazca-Antarctic-Phoenixslab windows beneath Patagonia and the Antarctic Peninsula. Tectonophysics 464 (1-4): 10-20.

Cande, S.C.; Leslie, R.B. 1986. Late Cenozoic tectonics of the Southern Chile trench. Journal of Geophysical Research 91: 471-496.

Cembrano, J.; Lavenu, A.; Reynolds, P.; Arancibia, G.; López, G.; Sanhueza, A. 2002. Late Cenozoic transpressional ductile deformation north of the Nazca-South America-Antarctica triple junction. Tectonophysics 354: 289-314.

Cotten, J.; Le Dez, A.; Bau, M.; Caroff, M.; Maury, R.C.; Dulski, P.; Fourcade, S.; Bohn, M.; Brousse, R. 1995. Origin of anomalous rare-earth elements and ytrium enrichments in subaereally exposed basalts: evidence from French Polynesia. Chemical Geology 119: 115-138.

Defant, M.J.; Richerson, M.; de Boer, J.Z.; Stewart, R.H.; Maury, R.C.; Bellon, H.; Drummond, M.S.; Feigenson, M.D.; Jackson, T.E. 1991. Dacite genesis via both slab melting and differentiation: Petrogenesis of La Yeguada Volcanic Complex, Panama. Journal of Petrology 32: 1101-1142.

D'Orazio, M.; Innocenti, F.; Manetti, P.; Tamponi, M.; Tonarini, S.; González-Ferrán, O.; Lahsen, A.; Omarini, 2003. The Quaternary calc-alkaline volcanism of the Patagonian Andes close to the Chile triple junction: geochemistry and petrogenesis of volcanic rocks from the Cay and Maca volcanoes (45°S, Chile). Journal of South American Earth Sciences 16 (4): 219-242.

Ellam, R.M.; Hawkesworth, C.J. 1988. Elemental and isotope variations in subduction related basalts: evidence for a three component model. Contributions to Mineralogy and Petrology 98: 72-80.

Escosteguy, L.; Dal Molin, C.; Franchi, M.; Geuna, S.; Lapido, O. 2002. Estratigrafía de la cuenca de los ríos El Zeballos y Jeinemeni, Noroeste de la provincia de Santa Cruz. *In* Congreso Geológico Argentino, No. 15, Actas 1: 653-658. El Calafate.

Espinoza, F.; Morata, D.; Pelleter, E.; Maury, R.C.; Suárez, M.; Lagabrielle, Y.; Polvée, M.; Bellon, H.; Cotten, J.; De la Cruz, R.; Guivel, C. 2005. Petrogenesis of the Eocene and Mio-Pliocene alkaline basaltic magmatism in Meseta Chile Chico, Southern Patagonia, Chile: evidence for the participation of two slab Windows. Lithos 82: 315-343.

Espinoza, F.; Morata, D.; Polvé, M.; Lagabrielle, Y.; Maury, R.C.; Guivel, C.; Cotten, J.; Bellon, H.; Suárez, M. 2008. Bimodal back-arc alkaline magmatism after ridge subduction: Pliocene felsic rocks from Central Patagonia (47°S). Lithos 101 (1-2): 191-217.

Feagle, J.G.; Bown, T.M.; Swisher, C.; Buckley, G.A. 1995. Age of the Pinturas and Santa Cruz Formations. *In* Congreso Argentino de Paleontología y Bioestratigrafía, No. 6, Actas 1: 129-135. Trelew, Argentina.

Flint, S.S.; Prior, D.J.; Agar, S.M.; Turner, P. 1994. Stratigraphic and structural evolution of the Tertiary Cosmelli Basin and its relationship to the Chile triple junction. Journal of the Geological Society of London 151: 251-268.

Foley, S.F.; Barth, M.G.; Jenner, G.A. 2000. Rutile/melt partition coefficients for trace elements and an assessment of the influence of rutile on the trace element characteristics of subduction zone magmas. Geochimica et Cosmochimica Acta 64 (5): 933-938.

Futa, K.; Stern, C.R. 1988. Sr and Nd isotopic and trace element composition of Quaternary volcanic centers of southern Andes. Earth and Planetary Science Letters 88: 253-263.

Gorring, M.; Kay, S. 2001. Mantle processes and sources of Neogene slab window magmas from southern Patagonia, Argentina. Journal of Petrology 42 (6): 1067-1094.

Gorring, M.L.; Kay, S.M.; Zeitler, P.K.; Ramos, V.A.; Rubiolo, D.; Fernández, M.I.; Panza, J.L. 1997. Neogene Patagonian plateau lavas: Continental magmas associated with ridge collision at the Chile Triple Junction. Tectonics 16: 1-17.

Gorring, M.; Singer, B.; Gowers, J.; Kay, S. 2003. Plio-Pleistocene basalts from the Meseta del Lago Buenos Aires, Argentina: evidence for asthenosphere-lithosphere interactions during slab window magmatism. Chemical Geology 193: 215-235.

Grove, T.L.; Elkind-Tanton, L.T.; Parman, S.W.; Chatterjee, N.; Müntener, O.; Gaetani, G.A. 2003. Fractional crystallization and mantle-melting controls on calc-alkaline differentiation trends. Contributions to Mineralogy and Petrology 145: 515-533.

Guivel, C.; Morata, D.; Pelleter, E.; Espinoza, F.; Maury, R.C.; Lagabrielle, Y.; Polvé, M.; Bellon, H.; Cotten, J.; Benoit, M.; Suárez, M.; De la Cruz, R. 2006. Miocene to Late Quaternary Patagonian basalts (46-47°S): Geochronometric and geochemical evidence for slab tearing due to active spreading ridge subduction: Journal of Volcanology and Geothermal Research 149: 346-370.

Gutscher, M.A.; Maury, R.C.; Eissen, J.-P.; Bourdon, E. 2000. Can slab melting be caused by flat subduction? Geology 28: 535-538.

Heintz, M.; Debayle, E.; Vauchez, A. 2005. Upper mantle structure of the South American continent and neighboring oceans from surface wave tomography. Tectonophysics 406: 115-139.

Hervé, F. 1993. Paleozoic metamorphic complexes in the Andes of Aysén, southern Chile (west of Occidentalia). *In* Proceedings of the First Circum-Pacific and Circum-Atlantic Terrane Conference: 64-65. Guanajuato, México.

Holland, T.J.B.; Blundy J. 1994. Non-ideal interactions in calcic amphiboles and their bearing on amphibole-plagioclase thermometry. Contribution to Mineralogy and Petrology 116: 433-447.

Irvine, T.N.; Baragar, W.R.A. 1971. A guide to the chemical classification of the common volcanic rocks. Canadian Journal of Earth Science 8: 523-548.

Jordan, T.; Burns, W.; Veiga, R.; Pángaro, F.; Copeland, P.; Kelley, S.; Mpodozis, C. 2001. Extension and basin formation in the Southern Andes caused by increased convergence rate: A Mid-Cenozoic trigger for the Andes. Tectonics 20: 308-324.

Kay, S.M.; Gordillo, C.E. 1994. Pocho volcanic rocks and the melting of depleted continental lithosphere above a shallowly dipping subduction zone in the Central Andes. Contributions to Mineralogy and Petrology 117: 25-44.

Kay, S.M.; Mpodozis, C. 2002. Magmatism as a probe to the Neogene shallowing of the Nazca plate beneath the modern Chilean flat-slab. Journal of South American Earth Sciences 15 (1): 39-57.

Kay, S.M.; Ramos, V. (editors) 2006. Evolution of an Andean margin: A tectonic and magmatic view from the Andes to the Neuquén Basin (35°-39°S lat). Geological Society of America Special Paper 407.

Kay, S.M.; Ramos, V.A.; Márquez, M. 1993. Evidence in Cerro Pampa volcanic rocks for slab-melting prior to ridge-collision in southern South America. Journal of Geology 101: 703-714.

Kay, S.M.; Mancilla, O.; Copeland, P. 2006. Evolution of the late Miocene Chachahuén volcanic complex at 37°S over a transient shallow subduction zone under the Neuquén Andes. *In* Evolution of an Andean margin: A tectonic and magmatic view from the Andes to the Neuquén Basin (35°-39°S lat) (Kay, S.M.; Ramos, V.; editors). Geological Society of America Special Paper 407: 215-246.

Kilian, R.; Behrmann, J. 2003. Geochemical constraints on the sources of Southern Chile Trench sediments and their recycling in arc magmas of the Southern Andes. Journal of the Geological Society of London 160: 57-70.

Lagabrielle, Y.; Suárez, M.; Rossello, E.A.; Hérail, G.; Martinod, J.; Régnier, M.; De la Cruz, R. 2004. Neogene to Quaternary tectonic evolution of the Patagonian Andes at the latitude of the Chile triple junction: Tectonophysics 385 (1-4): 211-241.

Lagabrielle, Y.; Bellón, H.; Espinoza, F.; Guivel, C.; Malavieille, J.; Maury, R.; Morata, D.; Polvé, M.; Rossello, E.; Suárez, M. 2006. Post-Pliocene Deformation and Uplift of the Patagonian Andes in response to the subduction of the active Chile Spreading Ridge (CSR). *In* Backbone of the Americas 4-2: 47. Mendoza, Argentina.

Lagabrielle, Y.; Suárez, M.; Malavieille, J.; Morata, D.; Espinoza, F.; Maury, R.C.; Scalabrino, B.; Barbero, L.; De la Cruz, R.; Rossello, E.; Bellon, H. 2007. Pliocene extensional tectonics in the Eastern Central Patagonian Cordillera: geochronological constraints and new field evidence. Terra Nova 19 (6): 413-424.

Le Bas, M.J.; Le Maitre, R.W.; Streckeisen, A.; Zanettin, B. 1986. A chemical classification of volcanic rocks based on the total alkali-silica diagram. Journal of Petrology 27: 745-750.

Linares, E.; González, R.R. 1990. Catálogo de edades radiométricas de la República Argentina 1957-1987. Asociación Geológica Argentina, Publicaciones Especiales Serie B, Didáctica y Complementaria 19: 1-628. Buenos Aires.

López-Escobar, L.; Kilian, R.; Kempton, P.; Tagiri, M. 1993. Petrography and geochemistry of Quaternary rocks from the Southern Volcanic Zone of the Andes between 41°30′ and 46°00′S, Chile. Revista Geológica de Chile 20 (1): 33-55.

Mahood, G.; Drake, R.E. 1982. K-Ar dating young rhyolitic rocks: a case study for the Sierra La Primavera, Jalisco, México. Geological Society of America Bulletin 93: 1232-1241.

Marshall, L.G.; Drake, R.E.; Curtis, G.H.; Butler, R.F.; Flanagan, K.M.; Naeser, C.W. 1986. Geochronology of type Santacrucian (middle Tertiary) land mammal age, Patagonia, Argentina. Journal of Geology 94: 449-457.

Michael, P.J. 1983. Emplacement and differentiation of Miocene plutons in the foothills of the southernmost Andes. Ph.D. Thesis (Unpublished), Columbia University: 367 p.

Morello, F.; San Ramón, M.; Prieto, A.; Stern, C.R. 2001. Nuevos antecedentes para una discusion arqueológica en torno a la obsidiana verde en Patagonia meridional. Anales del Instituto de la Patagonia 29: 129-148.

Morimoto, N.; Fabries, J.; Ferguson, A.K.; Ginzburg, I.V.; Ross, M.; Seifert, F.A.; Zussmann, J.; Aoki, K.; Gottardi, G. 1988. Nomenclature of piroxenes. American Mineralogist (173): 1123-1133.

Murdie, R.; Styles, P.; Prior, D.J.; Daniel, A.J. 2000. A new gravity map of southern Chile and its preliminary interpretation. Revista Geológica de Chile 27 (1): 49-63.

Nakamura, N. 1974. Determination of REE, Ba, Fe, Mg, Na and K in carbonaceous and ordinary chondrites. Geochimica Cosmochimica Acta (38): 757-775.

Panjasawatwong, Y.; Danyushevsky, L.V.; Crawford, A.J.; Harris, K.L. 1995. An experimental study of the effects of melt composition on plagioclase-melt equilibria at 5 and 10 kbar: implications for the origin of magmatic high-An plagioclase. Contributions to Mineralogy and Petrology 118 (4): 420-432.

Pankhurst, R.J.; Weaver, S.D.; Hervé, F.; Larrondo, P. 1999. Mesozoic-Cenozoic evolution of the North Patagonian Batholith in Aysén, southern Chile: Journal of the Geological Society 156: 673-694. London.

Parada, M.A.; Lahsen, A.; Palacios, C. 2000. The Miocene plutonic event of the Patagonian Batholith at 44°30'S: thermocronological and geobarometric evidence for melting of a rapidly exhumed lower crust. Transactions of the Royal Society of Edinburgh: Earth Sciences 91: 169-179.

Pardo-Casas, F.; Molnar, P. 1987. Relative motion of the Nazca (Farallón) and South American Plates since Late Cretaceous time. Tectonics 6: 233-248.

Pearce, J.A.; Peate, D.W. 1995. Tectonic implications of the composition of volcanic arc lavas. Annual Review of Earth and Planetary Sciences 23: 251-285.

Peccerillo, A.; Taylor, S.R. 1976. Geochemistry of Eocene Calc-Alkaline Volcanic Rocks from the Kastamonu Area, Northern Turkey. Contribution to Mineralogy and Petrology 58: 63-81.

Pin, C.; Telouk, P.; Imbert, J-L. 1995. Direct determination of the samarium: neodymium ratio in geological materials by inductively coupled plasma quadrupole mass spectrometry with cryogenic desolvation. Comparison with isotope dilution thermal ionization mass spectrometry. Journal of Analytical Atomic Spectrometry 10: 93-98.

Ramos, V.A. 1989. Andean foothills structures in northern Magallanes Basin, Argentina. American Association of Petroleum Geologist Bulletin 73: 887-903.

Ramos, V.A. 2002. El magmatismo neógeno de la Cordillera Patagónica. *In* Geología y Recursos Naturales de Santa Cruz (Haller, M.J; editor). Congreso Geológico Argentino, No. 15, Relatorio I (13): 187-199. El Calafate.

Ramos, V.A.; Folguera, A. 2009. Andean flat-slab subduction through time. Geological Society of London, Special Publications 327: 31-54.

Ramos, V.; Kay, S.M.; Singer, B.S. 2004. Las adakitas de la cordillera Patagónica: Nuevas evidencias geoquímicas y geocronológicas. Revista de la Asociación Geológica Argentina 59 (4): 693-706.

Ringwood, A.E. 1990. Slab-mantle interactions. 3. Petrogenesis of intraplate magmas and structure of the upper mantle. Chemical Geology 82 (3-4): 187-207.

Sánchez, A.; Hervé, F.; De Saint-Blanquat, M. 2008. Relations between plutonism in the back-arc region in southern Patagonia and Chile Rise subduction: A geochronological review. *In* International Symposium on Andean Geodynamics: 485-488. Nice.

Schmidt, M.W.; Dardon, A.; Chazot, G.; Vanucci, R. 2004. The dependance of Nb and Ta rutile-melt partitioning on melt composition and Nb/Ta fractionation during subduction processes. Earth and Planetary Science Letters 226: 415-432.

Somoza, R. 1998. Updated Nazca (Farallon)-South America relative motions during the last 40 my: implications for mountain building in the central Andean region. Journal of South American Earth Sciences 11: 211-215.

Steiger, R.H.; Jäger, E. 1977. Subcommission on geochronology: convention on the use of decay constants in geo- and cosmochronology. Earth and Planetary Science Letters 36: 359-362.

Stern, C.R.; Frey. F.A.; Futa, K.; Zartman, R.E.; Peng, Z.; Kyser, T.K. 1990. Trace-element and Sr, Nd, Pb and O isotopic composition of Pliocene and Quaternary basalts of the Patagonian Plateau lavas of southernmost South America. Contribution to Mineralogy and Petrology 104: 294-308.

Suárez, M.; De la Cruz, R. 2001. Jurassic to Miocene K-Ar dates from eastern central Patagonian Cordillera plutons, Chile (45°-48°S). Geological Magazine 138 (1): 53-66.

Suárez, M.; De la Cruz, R.; Bell, C.M. 2000. Timing and origin of deformation along the Patagonian fold and thrust belt. Geological Magazine 137: 345-353.

Sun, S.; McDonough, W.F. 1989. Chemical and isotopic systematics of oceanic basalts; implications for mantle composition and processes. *In* Magmatism in the Ocean Basins (Saunders, A.D.; Norry, J.M.; editors). Geological Society of London, Special Publication 42: 313-345.

Tatsumi, Y.; Eggins, S. 1995. Subduction Zone magmatism. Blackwell Publishing: 224 p.

Thomson, S.N.; Hervé, F.; Stöckhert, B. 2001. Mesozoic-Cenozoic denudation history of the Patagonian Andes (southern Chile) and its correlation to different subduction processes. Tectonics 20: 693-711.

Thorkelson, D.J.; Breitsprecher, K. 2005. Partial melting of slab window margins: genesis of adakitic and non-adakitic magmas. Lithos 79: 25-41.

Ugarte, F. 1956. El Grupo Río Zeballos. Revista de la Asociación Geológica Argentina 11 (3): 202-216.

Vroon, P.Z.; van Bergen, M.J.; Klaver, G.J.; White, W.M. 1995. Strontium, neodymium, and lead isotopic and trace-element signatures of the East indonesian sediments: provenance and implications for banda arc magma genesis. Geochimica et Cosmochimica Acta 59 (12): 2573-2598.

Yáñez, G.A.; Ramiro, C.; von Huene, R.; Díaz, J. 2001. Magnetic anomaly interpretation across the southern central Andes (32°-34°S): The role of the Juan Fernández Ridge in the late Tertiary evolution of the margin. Journal of Geophysical Research 106: 6325-6345.

Manuscript received: October 10, 2009; revised/accepted: May 11, 2010.